Article

Cell Reports

SorCS2 Controls Functional Expression of Amino Acid Transporter EAAT3 and Protects Neurons from Oxidative Stress and Epilepsy-Induced Pathology

Graphical Abstract

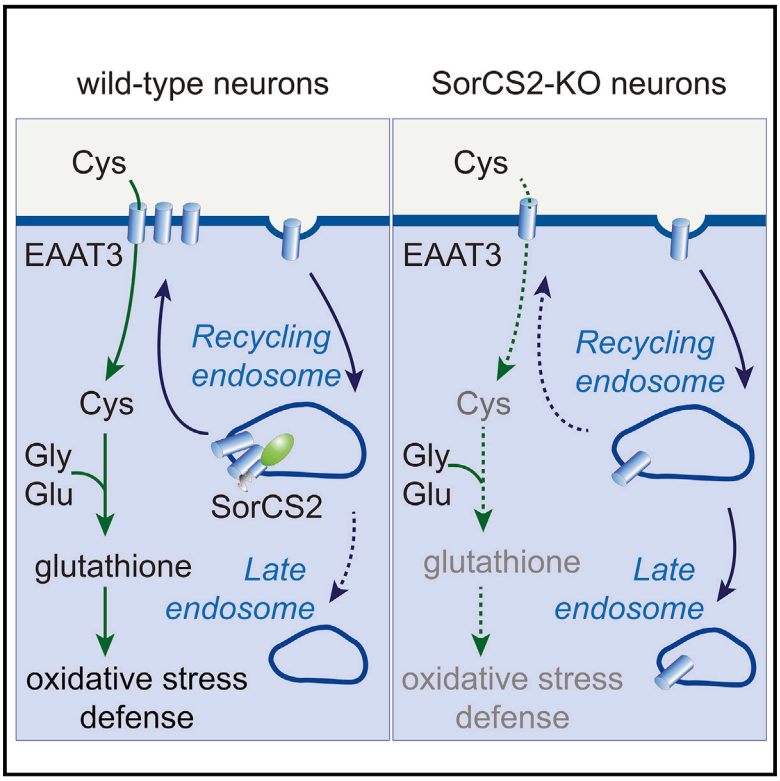

Authors

Anna R. Malik, Kinga Szydlowska, Karolina Nizinska, ..., Katarzyna Lukasiuk, Eleonora Aronica, Thomas E. Willnow

Correspondence

anna.malik@mdc-berlin.de (A.R.M.), willnow@mdc-berlin.de (T.E.W.)

In Brief

Malik et al. uncover a mechanism crucial for neuronal oxidative stress defense. They show that sorting receptor SorCS2 facilitates cell surface expression of cysteine transporter EAAT3. Loss of *Sorcs2* impairs neuronal cysteine import and glutathione production, increases vulnerability to oxidative damage, and aggravates epilepsy-induced brain pathology and death in mice.

Highlights

- SorCS2 is upregulated in neurons of human and mouse epileptic brains
- SorCS2 protects from oxidative damage and death in a mouse model of epilepsy
- Cysteine transporter EAAT3 is a target for SorCS2-dependent intracellular sorting
- SorCS2 loss impairs neuronal cysteine import and reduces glutathione levels

Malik et al., 2019, Cell Reports *26*, 2792–2804
March 5, 2019
https://doi.org/10.1016/j.celrep.2019.02.027

CellPress

OPEN ACCESS
CellPress

Cell Reports
Article

SorCS2 Controls Functional Expression of Amino Acid Transporter EAAT3 and Protects Neurons from Oxidative Stress and Epilepsy-Induced Pathology

Anna R. Malik,[1,*] Kinga Szydlowska,[2] Karolina Nizinska,[2] Antonino Asaro,[1] Erwin A. van Vliet,[3,4] Oliver Popp,[1] Gunnar Dittmar,[5] Raphaela Fritsche-Guenther,[1,6] Jennifer A. Kirwan,[1,6] Anders Nykjaer,[7] Katarzyna Lukasiuk,[2] Eleonora Aronica,[3,8] and Thomas E. Willnow[1,9,*]

[1]Max-Delbrueck-Center for Molecular Medicine, 13125 Berlin, Germany
[2]Nencki Institute of Experimental Biology, Polish Academy of Sciences, 02-093 Warsaw, Poland
[3]Department of (Neuro)Pathology, Academic Medical Center, University of Amsterdam, 1105AZ Amsterdam, the Netherlands
[4]Swammerdam Institute for Life Sciences, University of Amsterdam, 1098 XH, Amsterdam, the Netherlands
[5]Department of Oncology, Luxembourg Institute of Health, 1445 Strassen, Luxembourg
[6]Berlin Institute of Health Metabolomics Platform, 10178 Berlin, Germany
[7]MIND Center, Danish Research Institute of Translational Neuroscience - DANDRITE, The Danish Research Foundation Center PROMEMO, Departments of Biomedicine, Aarhus University, and Neurosurgery, Aarhus University Hospital, 8000C Aarhus, Denmark
[8]Stichting Epilepsie Instellingen Nederland (SEIN), 2103 SW Heemstede, the Netherlands
[9]Lead Contact
*Correspondence: anna.malik@mdc-berlin.de (A.R.M.), willnow@mdc-berlin.de (T.E.W.)
https://doi.org/10.1016/j.celrep.2019.02.027

SUMMARY

VPS10P domain receptors emerge as central regulators of intracellular protein sorting in neurons with relevance for various brain pathologies. Here, we identified a role for the family member SorCS2 in protection of neurons from oxidative stress and epilepsy-induced cell death. We show that SorCS2 acts as sorting receptor that sustains cell surface expression of the neuronal amino acid transporter EAAT3 to facilitate import of cysteine, required for synthesis of the reactive oxygen species scavenger glutathione. Lack of SorCS2 causes depletion of EAAT3 from the plasma membrane and impairs neuronal cysteine uptake. As a consequence, SorCS2-deficient mice exhibit oxidative brain damage that coincides with enhanced neuronal cell death and increased mortality during epilepsy. Our findings highlight a protective role for SorCS2 in neuronal stress response and provide a possible explanation for upregulation of this receptor seen in surviving neurons of the human epileptic brain.

INTRODUCTION

Sorting of proteins to their correct target sites is fundamental for maintaining proper cell functions. Intracellular protein sorting is particularly challenging for neurons, composed of diverse subcellular compartments in cell soma, dendrites, and axons. Not surprisingly, aberrant neuronal protein sorting has therefore been recognized as the underlying cause of many devastating brain pathologies (Wang et al., 2013). In recent years, the characterization of a class of intracellular sorting receptors, termed VPS10P domain receptors, has shed light on the mechanisms that govern protein sorting in neurons. VPS10P domain receptors encompass a group of five structurally related type 1 transmembrane proteins expressed in neurons of the central and peripheral nervous systems. Gene family members are SORLA, sortilin, as well as SorCS1, SorCS2, and SorCS3 (Willnow et al., 2008). As a common feature, VPS10P domain receptors act as sorting receptors that direct cargo proteins between Golgi, cell surface, and endosomes. One of their ascribed functions is the ability to move signaling receptors to and from the cell surface, providing control of neuronal signal reception. Examples of such activity include sorting of neurotrophin receptors by sortilin (Vaegter et al., 2011) and SorCS1 and SorCS3 (Subkhangulova et al., 2018).

Recently, VPS10P domain receptors have received growing attention because of their relevance for disorders of the human brain. Thus, encoding genes have been associated with psychiatric diseases, including *SORCS1* with attention-deficit hyperactivity disorder (Lionel et al., 2011) and *SORCS2* with bipolar disorder (Baum et al., 2008; Ollila et al., 2009) and schizophrenia (Christoforou et al., 2011). Although the molecular mechanisms whereby VPS10P domain receptors affect brain diseases are still not fully resolved, faulty protein transport has been identified as one of the underlying reasons, as shown for SORLA as a sorting receptor for the amyloid precursor protein in Alzheimer's disease (Andersen et al., 2005; Offe et al., 2006).

As well as by genetic association, VPS10P domain receptors have also been implicated in brain pathologies by expression studies identifying altered receptor levels in the diseased brains of patients or animal models (Andersen et al., 2005; Reitz et al., 2013; Saadipour et al., 2013). With relevance to this study, *Sorcs2* was identified as a gene strongly upregulated in an experimental mouse model of temporal lobe epilepsy (TLE), linking this receptor with neuropathologies associated with brain seizures (VonDran et al., 2014). However, the underlying mechanism of SorCS2 action, and whether it bears relevance for epilepsy in humans, remained unclear. Combining unbiased

proteomic screens for SorCS2 targets with studies in receptor-deficient mouse models and in patients with TLE, we now identified the function of this receptor in trafficking of the neuronal glutamate and cysteine transporter EAAT3. SorCS2-facilitated exposure of EAAT3 on the cell surface promotes uptake of cysteine, the precursor to produce glutathione, a scavenger for reactive oxygen species, and it protects neurons from oxidative stress induced by seizures. Jointly, these findings uncovered the significance of directed protein sorting for neuronal stress response and as a neuroprotective pathway in epilepsy.

RESULTS

SorCS2 Is Upregulated in the Epileptic Human Brain and Plays a Protective Role in an Experimental Model of TLE

Epilepsy is a complex chronic brain disorder characterized by seizures, leading to circuit reorganization and neuronal cell loss. Pathological features of the human disease can be recapitulated in mouse models of epilepsy involving the administration of chemoconvulsants, such as pilocarpine or pentylenetetrazol (PTZ). With relevance to this study, SorCS2 emerged as one of the proteins strongly upregulated in neurons of the hippocampus 3 days after status epilepticus induced by pilocarpine. Increased receptor expression was particularly evident in the hilus and cornus ammonis 2 (CA2) region (VonDran et al., 2014). To substantiate the relevance of this observation for human brain pathology, we tested the expression pattern of SorCS2 in the healthy and in the epileptic human hippocampus with hippocampal sclerosis (HS) (Figure 1A). In healthy tissue, we observed robust SorCS2 expression in neurons of the hippocampus, in agreement with its reported expression pattern in the murine brain (Hermey et al., 2004) (Figure 1A, top left). In human TLE-HS tissue, severe neuronal cell loss was visible in all hippocampal regions, with the exception of CA2, which is particularly resistant to epilepsy-driven degeneration (Figure 1A, top right) (Steve et al., 2014). Strikingly, surviving neurons in the CA2 region of TLE-HS tissue samples showed a substantial increase in SorCS2 levels, suggesting a role for SorCS2 in preventing neuron loss in the course of epilepsy (Figure 1A, bottom).

To investigate SorCS2 functions in epilepsy, we turned to a PTZ-induced kindling paradigm applied to mice either wild-type (WT) or genetically deficient for *Sorcs2* (referred to as S2KO [SorCS2 knockout]) (Glerup et al., 2014). In this chronic epilepsy model, mice were subjected to a sub-convulsive dose of PTZ three times a week for 5 weeks and scored for the severity of their seizures (0–5; 6 in case of death). Over time, mice repeatedly challenged with PTZ develop convulsions of increasing severity (Becker et al., 1992). As seen for the epileptic human brain (Figure 1A), we also observed substantially increased levels of SorCS2 in the CA2 region of the hippocampus in PTZ-kindled WT mice using immunohistochemistry (Figure 1B). Overall, S2KO mice presented a kindling phenotype comparable with that of WT animals (Figures 1C and S1). Also, seizures resulting from the first administration of PTZ, reflecting the acute response to the stimulus, did not differ between SorCS2-deficient and control animals (Figure 1C). However, we observed a striking difference in the mortality rate of the two genotype groups during the course of the kindling experiment with the mortality rate being higher in S2KO compared with WT mice (Figure 1D). After developing strong seizures (score 5), SorCS2-deficient mice died within the next three sessions on average, whereas WT mice survived for approximately six more sessions (Figure 1E). This observation indicated that SorCS2-deficient mice were prone to developing irreversible pathological changes during kindling that eventually led to their death.

Loss of SorCS2 Aggravates Cell Death and Oxidative Damage in a Murine Model of Epilepsy

Neuronal cell death caused by seizures has a critical impact on the brain function (Dingledine et al., 2014). To test whether the increased mortality of S2KO mice in the PTZ kindling paradigm was accompanied by aggravated neuronal cell loss, we assessed the number of dying cells in the hippocampi of WT and S2KO mice by TUNEL staining at the end of the PTZ kindling experiment. The number of TUNEL-positive cells was significantly higher in CA2/3 regions of S2KO hippocampi compared with WT tissue (Figures 2A and 2B). Because the kindling phenotype and the extent of seizures after the first PTZ dose were comparable between the genotypes, we reasoned that the aggravated cell death in S2KO hippocampi was not due to an overall increase in responsiveness to PTZ. Possibly, repeated epileptic seizures may lead to secondary changes in brain functions that were more pronounced in the S2KO compared with the WT brain. Because oxidative stress is a feature of epilepsy that likely contributes to epilepsy-associated cell death (Shin et al., 2011), we tested the levels of the oxidative stress marker 8-hydroxy-2′-deoxyguanosine (8OHdG) in mouse hippocampi after PTZ kindling. 8OHdG is one of the predominant forms of free radical-induced oxidative lesions in nuclear and mtDNA (Valavanidis et al., 2009). 8OHdG immunoreactivity was significantly increased in S2KO hippocampi compared with WT tissues, both in the dentate gyrus (DG) and the CA region (Figures 2C and 2D). This observation suggested that brain damage induced in S2KO mice by PTZ kindling might be related to increased susceptibility to oxidative stress.

In support of this concept, we documented an aggravated response to oxidative stress in primary SorCS2-deficient neurons, despite their normal activation by classical neuronal stimulation. Thus, S2KO neurons responded normally to treatment with the GABA-A receptor antagonist bicuculline, as reflected by a similar extent of p-ERK induction in WT and S2KO neurons (Figures 3A and 3B). In contrast, treatment with the oxidant H_2O_2 triggered an increase in levels of the oxidative stress marker heme oxygenase-1 (HO-1) that was significantly more pronounced in S2KO than in WT neurons (Figures 3C and 3D). Oxidative stress was accompanied by a transient increase in SorCS2 levels in WT neurons (Figures 3E and 3F), supporting involvement of SorCS2 in stress response pathways.

Neuronal Surface Proteome Is Altered in S2KO Neurons

To elucidate SorCS2-dependent processes protecting neurons from oxidative stress, we applied an unbiased proteomics approach to identify molecular targets of SorCS2 in the neuronal surface proteome. This approach was based on the established role of VPS10P domain receptors in sorting proteins to and from the neuronal cell surface and on the documented alterations in

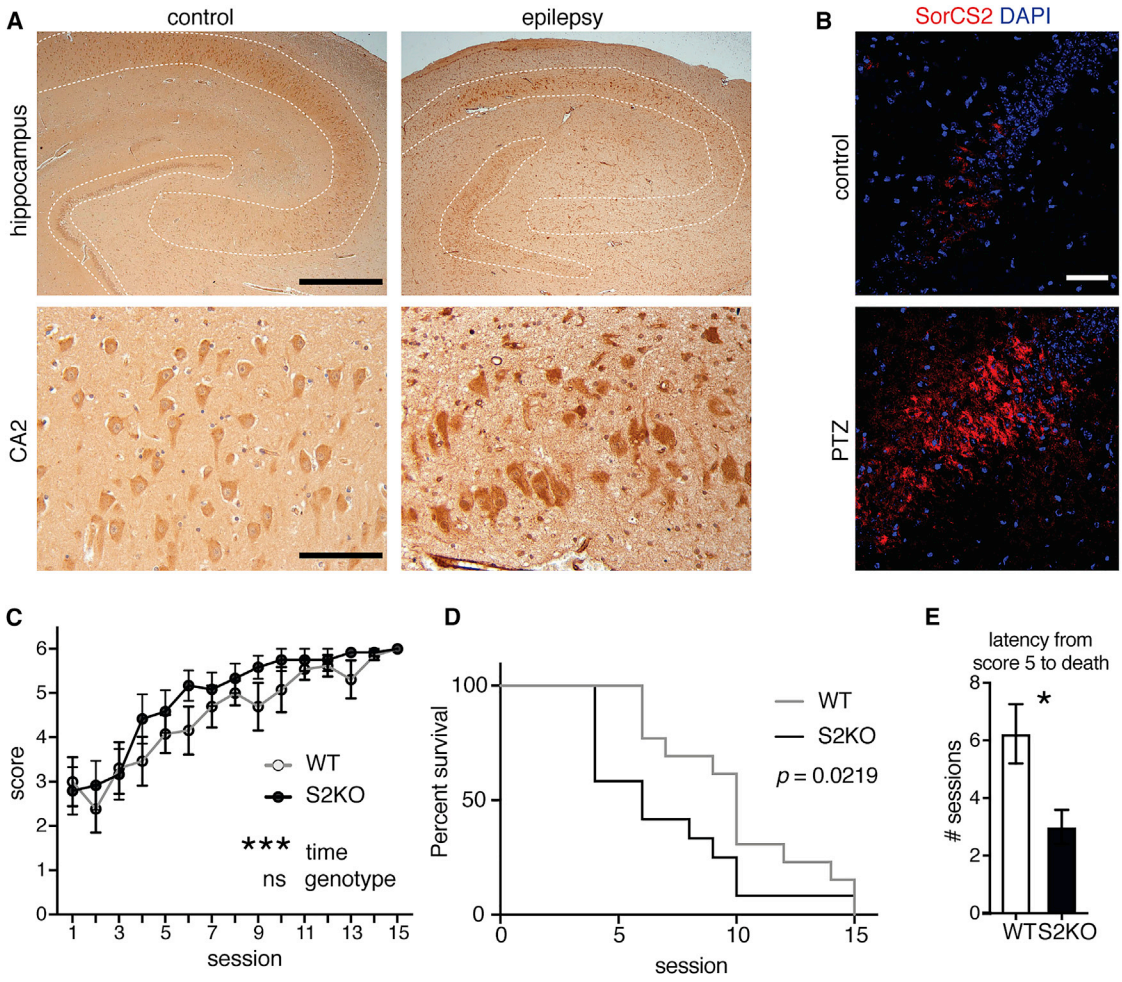

Figure 1. SorCS2 Is Upregulated in the Epileptic Human Brain and Plays a Protective Role in an Experimental Model of Temporal Lobe Epilepsy

(A) SorCS2 immunostaining in the human control hippocampus and in the hippocampus of a patient with TLE and hippocampal sclerosis. CA and DG regions are indicted by white dotted lines. Overviews (above) and higher magnifications of CA2 regions (below) are shown. Scale bars, overview, 1 mm; CA2 region, 100 μm. See also Table S1.

(B) SorCS2 immunostaining (red) in the CA2 region of the hippocampus of control and PTZ-kindled wild-type mice. Sections are counterstained with DAPI. Scale bar, 50 μm.

(C–E) Results of PTZ kindling experiments. Mice were injected with PTZ three times a week, as detailed in STAR Methods. n = 12 or 13 mice per genotype. See also Figure S1.

(C) Seizure scores (from 0 [no seizure] to 5; 6 indicates death) in the function of time. Mean value ± SEM. ns, not significant. ***$p < 0.001$ (two-way repeated-measures ANOVA).

(D) Survival curves in course of the PTZ kindling experiment. $p = 0.0219$ (Gehan-Breslow-Wilcoxon test).

(E) Latency (number of sessions) from score 5 to death for WT and S2KO mice. Mean value ± SEM. *$p < 0.05$ (unpaired t test).

cargo exposure on the surface of cells lacking individual VPS10P domain receptors (Mazella et al., 2010; Rohe et al., 2013). We had applied this strategy successfully before to identify ligands for SorCS1 and SorCS3 (Subkhangulova et al., 2018). Here, neuronal cell surface proteins in WT and S2KO primary neurons were purified and subjected to quantitative label-free mass spectrometry analysis (Figure 4A). In this experiment, we uncovered multiple proteins with altered abundance in the neuronal cell surface fraction upon loss of SorCS2 (Figure 4B; Tables S2 and S3). Proteins with decreased cell surface exposure in mutant neurons included SorCS2 (Figure 4B; Table S2), substantiating our strategy for identifying alterations in the neuronal cell surface proteome. Among the hits with altered plasma membrane exposure, we identified cell surface receptors, channels, and transporters, as well as proteins implicated in intracellular trafficking processes (Table S2). These hits represent bona fide cell membrane proteins and membrane-associated proteins, as well as proteins possibly included in the cell surface fraction as a result of their interaction with cell surface proteins.

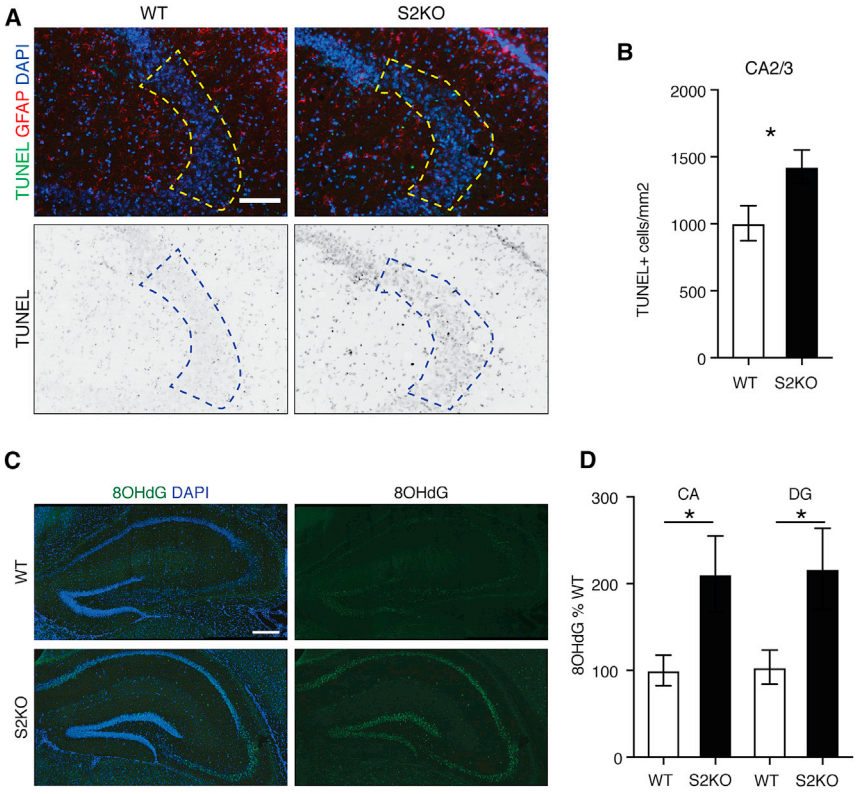

Figure 2. Loss of SorCS2 Aggravates Cell Death and Oxidative Stress Response in Murine Epilepsy Model

(A) TUNEL staining (green) in the CA2/3 region of the hippocampus of WT or S2KO mice after PTZ kindling. GFAP (red) marks astrocytes. Sections are counterstained with DAPI. Dashed lines indicate the areas used for quantification. Scale bar, 100 μm.

(B) Quantification of TUNEL-positive cells in the CA2/3 area. Mean ± SEM. n = 10 or 11 mice per genotype. *p < 0.05 (unpaired t test).

(C) Immunostaining for oxidative stress marker 8OHdG (green) in hippocampi of WT and S2KO mice after PTZ kindling. Sections are counterstained with DAPI. Scale bar, 250 μm.

(D) 8OHdG immunostaining intensity in the CA1–3 regions (CA) and dentate gyrus (DG) of WT and S2KO mice after PTZ kindling. Mean ± SEM. n = 12 or 13 mice per genotype. *p < 0.05 (unpaired t test).

Interestingly, two hits in our proteome screen, namely, JWA and mGlur3, were implicated in oxidative stress response. JWA is induced in cells in response to oxidative stress (Chen et al., 2007) and is implicated in regulation of the synthesis of the reactive oxygen species (ROS) scavenger glutathione (Watabe et al., 2008). Metabotropic glutamate receptors (mGlurs) also play a role in protection from oxidative stress, as activation of mGlur2 and mGlur3 increases synthesis of glutathione in dorsal root ganglion neurons (Berent-Spillson and Russell, 2007). We confirmed increased levels of JWA in the S2KO mouse brain (Figures 4C and 4D), as well as an increase in mGlur2/3 protein in SorCS2-deficient primary neurons (Figures S2A and S2B) and brain tissue (Figures S2D and S2E), substantiating the results of our proteome screen. An increase in mGlur3 expression in S2KO mice was already seen at the transcript level in both primary neurons and in brain (Figures S2C and S2F), while JWA mRNA levels remained unchanged comparing the two genotypes (Figures 4E and 4F). As we did not observe co-immunoprecipitation (coIP) of JWA or mGlur3 with SorCS2 (Figure S2G), we reasoned that alterations in the levels of these two proteins likely reflected secondary consequences of SorCS2 loss.

SorCS2 Colocalizes and Interacts with the Glutamate and Cysteine Transporter EAAT3

So far, our data pointed to alterations in glutamatergic and oxidative stress response systems in S2KO neurons. Both systems are mechanistically linked, as glutamate is not only a neurotransmitter but also a substrate for synthesis of glutathione, the main cellular ROS scavenger. Synthesis of glutathione requires two additional amino acids, glycine and cysteine. Importantly, glutamate and cysteine are imported into neurons by the same amino acid transporter excitatory amino acid transporter 3 (EAAT3; or excitatory amino acid carrier 1 [EAAC1]) (Chen and Swanson, 2003). Of note, JWA modulates trafficking and function of EAAT3 (Lin et al., 2001; Ruggiero et al., 2008), while activation of mGlur2/3 increased EAAT3 levels in glioma cells (Aronica et al., 2003), providing a mechanistic link of this amino acid transporter to hits in our proteome screen.

Next, we tested whether EAAT3 may represent a direct target of SorCS2-dependent sorting in neurons. In support of this hypothesis, expression patterns for SorCS2 and EAAT3 largely overlapped in the mouse brain on the cellular level, particularly in the pyramidal neurons of the cortex and in neurons of CA2 and DG of the hippocampus (Figure 4G). EAAT3 is expressed both in excitatory and in inhibitory GABAergic neurons (Conti et al., 1998). However, we did not observe SorCS2 expression in GABAergic, GAD67-positive neurons, neither in the mouse brain (Figure S3A) nor in neuronal cultures (Figure S3B), suggesting that co-expression of EAAT3 and SorCS2 occurs in excitatory neurons. In hippocampal neurons and rat C6 glioma cells, immunosignals for both proteins colocalized in intracellular vesicles, supporting a role for SorCS2 in trafficking of EAAT3 (Figure 4H).

To substantiate EAAT3 as a target for SorCS2-mediated sorting, we tested interaction of the two proteins by coIP. Direct interaction was documented by coIP of EAAT3 with GFP-tagged SorCS2 (SorCS2-GFP) in CHO cells (Figure 4I). No coIP of EAAT3 was seen with the control protein GFP-tagged β-galactosidase (βG) (Figure 4I). We confirmed EAAT3 and SorCS2 interaction by coIP of the endogenous proteins from mouse hippocampal lysates of WT mice using anti-SorCS2 antisera (Figure 4J). No IP of EAAT3 was seen using non-immune IgG or S2KO hippocampal lysates (Figure 4J).

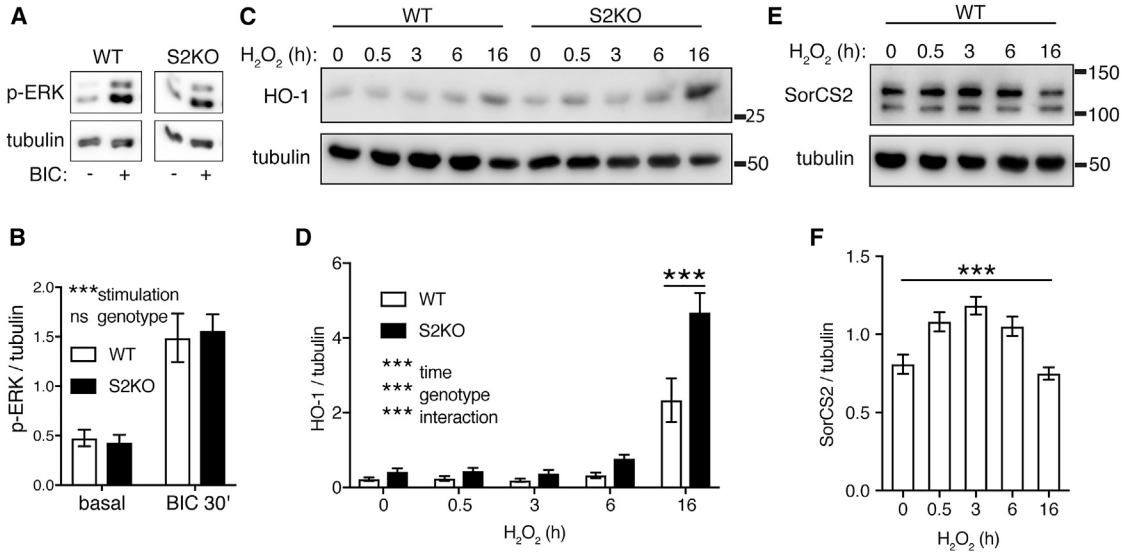

Figure 3. Loss of SorCS2 Aggravates Oxidative Stress Response in Primary Neurons

(A and B) Western blot analysis (A) of p-ERK levels in cell lysates after stimulation of primary WT and S2KO neurons with 20 μM bicuculline (BIC) for 30 min and quantification thereof (B). Tubulin served as a loading control. Mean ± SEM. n = 6 or 7 independent neuronal preparations per genotype. ns, not significant. ***p < 0.001 (two-way ANOVA).

(C and D) Western blot analysis (C) of HO-1 levels in cell lysates after treatment of primary WT and S2KO neurons with 200 μM H_2O_2 and quantification thereof (D). Tubulin served as a loading control. Mean ± SEM. n = 9 independent neuronal preparations per genotype. ***p < 0.001 (two-way ANOVA with Sidak's multiple-comparisons test).

(E and F) Western blot analysis (E) of SorCS2 levels in cell lysates after treatment of primary WT neurons with 200 μM H_2O_2 and quantification thereof (F). Tubulin serves as a loading control. Mean ± SEM. n = 9 independent neuronal preparations. ***p < 0.001 (one-way ANOVA).

In (A)–(F) mixed cortical-hippocampal cultures were used.

Loss of SorCS2 Leads to Missorting of EAAT3 in Neurons

To further substantiate EAAT3 as a target of sorting by SorCS2, we studied levels and subcellular distribution of EAAT3 in primary neurons from WT and S2KO mice. Specifically, we compared the total levels as well as the levels of EAAT3 in the cell surface fraction using western blot analysis. During cell lysate processing, EAAT3 tends to form aggregates that manifest as higher molecular mass bands in addition to the monomer (González et al., 2002; Danbolt et al., 2016). Consistent with this notion, EAAT3 was seen as both monomeric and aggregated forms in total cell lysate (Figure 5A, left) and in aggregated form in the surface fraction (Figure 5A, right). To exclude any bias from different affinities of the antisera for monomer versus aggregates, we quantified signal intensities for both forms of the protein separately as well as the total amount of EAAT3 present in the samples.

Levels of EAAT3 in the total lysate and in the cell surface fraction were significantly decreased in S2KO compared with WT neurons (Figures 5A and 5B). This decrease was observed for the total (aggregated) EAAT3 in the cell surface fraction, as well as for monomeric and total EAAT3 in the neuronal lysate (Figure 5B). We corroborated these findings in an alternative cell model by transient knockdown of SorCS2 in the C6 glioma cell line. Also for C6 cells, we observed monomeric and aggregated EAAT3 in cell lysates. SorCS2 depletion in C6 cells led to a significant decrease in the levels of aggregated and total EAAT3 (Figures 5D and 5E).

Finally, we substantiated the impact of SorCS2 deficiency on the subcellular distribution of EAAT3 in the brain by performing subcellular fractionation of murine brain lysates (Figure S4A). No aggregation of EAAT3 occurred when processing tissue lysates. Thus, in this and all subsequent studies using mouse brain tissue, only monomeric forms of EAAT3 were detected and quantified. Using western blot analyses, we detected EAAT3 in fractions P2 (crude membranes including the plasma membrane) and P3 (intracellular vesicles) (Figure S4B). In refined fractionations, EAAT3 localized to the extrasynaptic membranes (containing the plasma membrane) (Figure S4C) and to the synaptosomal fraction (Figure S4D), but not the post-synaptic density (PSD1; Figure S4D). SorCS2 showed the same subcellular distribution, with an obvious enrichment in the intracellular vesicle fraction P3 (Figures S4B–S4D). In agreement with these findings, immunostaining in primary hippocampal neurons located EAAT3 and SorCS2 to early endosomes and recycling endosomes, characterized by Rab5 and Rab11, respectively (Figure S4E). Comparing genotypes, levels of EAAT3 in the intracellular vesicle fraction P3 were significantly lower in S2KO compared with WT brain tissue (Figures 5F and 5G). This fraction contained Rab11-positive recycling endosomes (Figure S4B) that are central to the intracellular sorting and cell surface targeting of EAAT3 (González et al., 2007; Su et al., 2016). Loss of SorCS2 did not affect the levels of *Eaat3* transcript in primary neurons (Figure 5C) or brain cortex or hippocampus (Figure 5H). Taken together, these findings argued that alterations in levels and subcellular distribution

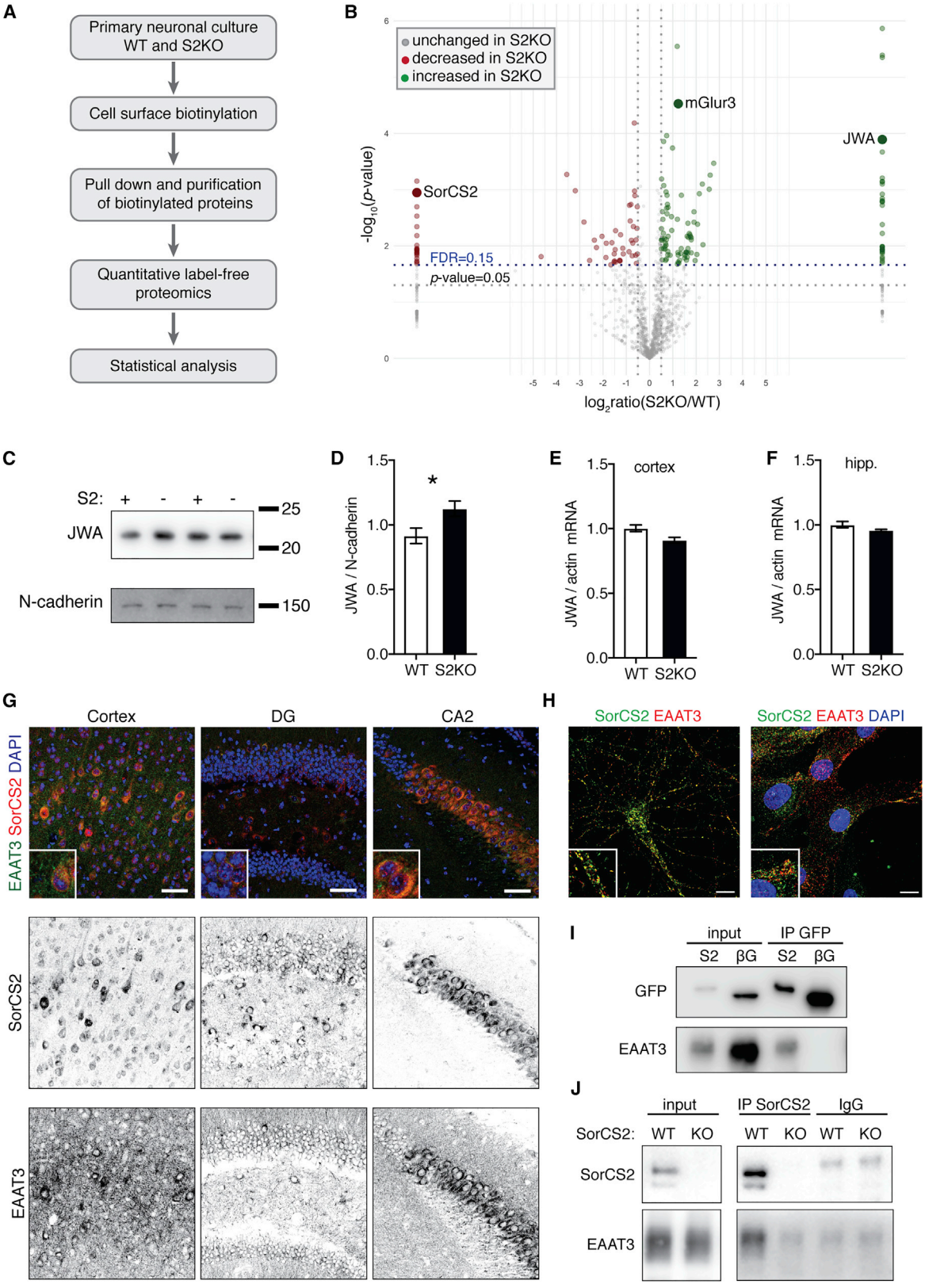

(legend on next page)

of EAAT3 in SorCS2-deficient neurons were caused by post-transcriptional perturbation, possibly by aberrant protein sorting.

SorCS2 Deficiency Targets EAAT3 to Late Endosomes

Loss of SorCS2 resulted in decreased cell surface exposure of EAAT3 in cultured neurons (Figures 5A and 5B) and in a decreased EAAT3 content in the intracellular vesicles fraction P3 (Figures 5F and 5G). Using immunocytochemistry, we explored the alternative fate of EAAT3 molecules in SorCS2-deficient primary neurons. We observed that the fraction of EAAT3 colocalizing with the late endosome marker Rab7 was significantly larger in primary S2KO neurons compared with WT cells (Figures 6A and 6B). To test whether missorting of EAAT3 to late endosomes in SorCS2 mutant neurons may promote lysosomal catabolism of the transporter, we quantified the amount of EAAT3 in the cell surface fraction of cells treated with lysosomal inhibitors. Blocking lysosomal proteolysis caused a significant increase in cell surface levels of EAAT3, indicating that lysosomal catabolism contributes to the decrease in EAAT3 levels in S2KO neurons (Figures 6C and 6D).

SorCS2 Promotes Cysteine Import into Neurons

To evaluate the impact of missorting on EAAT3 activity, we measured glutamate and cysteine uptake into primary neurons from WT and SorCS2-deficient mice. [S35]-labeled cysteine or [H3]-labeled glutamate were applied to cultured WT and S2KO neurons, and their intracellular content was assayed over time. Because EAAT3 is a sodium-dependent transporter, we performed parallel assays in Na-containing (Na^+) and Na-deprived (Na^-) buffer to control for the contribution of Na-independent transport to glutamate and cysteine uptake. No substantial contribution of Na-independent mechanisms to glutamate import into cultured neurons was noted (7% of total glutamate uptake at 6 min; Figure 6E). For cysteine, Na-independent transport accounted for 24% of total uptake at 6 min (Figure 6F). Therefore, in subsequent experiments we corrected for its contribution to cysteine import to exclusively quantify the Na-dependent transport activity. Comparing WT and S2KO neurons, glutamate uptake did not show any difference (Figure 6G), likely explained by the fact that cultured neurons also express other Na-dependent glutamate transporters (Chen and Swanson, 2003). By contrast, Na-dependent cysteine import was significantly decreased in S2KO neurons (Figure 6H), documenting a functional consequence of EAAT3 missorting in SorCS2-deficient neurons. Impaired EAAT3-dependent cysteine import into neurons results in reduced glutathione synthesis in this cell type (Aoyama et al., 2006). In line with this concept, glutathione levels in the CA2 region of SorCS2-deficient mice were significantly reduced compared with WT animals (Figures 6I and 6J) as shown by immunodetection of the glutathione-*N*-ethylmaleimide adducts (GSH:NEM) (Escartin et al., 2011).

Subcellular Distribution of EAAT3 Is Dynamically Regulated during Epilepsy in a SorCS2-Dependent Manner

SorCS2-dependent cell surface exposure of EAAT3 promotes cysteine import and glutathione synthesis in neurons (Figures 6H–6J). To query whether this interaction bares relevance for neuroprotection, we tested the functional interaction of both proteins in response to oxidative stress *in vitro* and *in vivo*. In primary neurons, H_2O_2 treatment increased colocalization of EAAT3 with SorCS2 in intracellular vesicles (Figures 7A and 7B), supporting the idea that EAAT3 might be dynamically sorted by SorCS2 upon oxidative stress. We corroborated the responsiveness of EAAT3 to stress by documenting a dramatically increased immunosignal for the transporter in the surviving neurons of the human epileptic hippocampus, in particular in the CA2 region (Figure 7C), as previously shown for SorCS2 (Figure 1A). To test whether dynamic sorting of EAAT3 also occurs in epilepsy and depends on SorCS2, we assayed the subcellular distribution of EAAT3 after PTZ kindling using subcellular fractionations of WT and SorCS2-deficient brain tissues. In WT brains, we observed a redistribution of EAAT3 from the intracellular vesicle fraction P3 (including $Rab11^+$ endosomes) to the extrasynaptic membranes fraction (containing the plasma membrane) following kindling compared with the control condition (Figures 7D and 7E). No such shift from P3 to the extrasynaptic membranes fraction was seen in mouse brains lacking SorCS2 (Figures 7D and 7E).

In conclusion, we identified a role for SorCS2 in dynamic intracellular sorting of EAAT3 in response to oxidative stress, a pathway that facilitates neuronal uptake of cysteine required for production of glutathione. Loss of SorCS2 impairs EAAT3-dependent uptake of cysteine and reduces glutathione levels, which coincides with a compromised protection against epilepsy-induced oxidative stress and neuronal cell death.

Figure 4. Cell Surface Proteomics Reveals Targets for SorCS2-Dependent Sorting

(A) Workflow of surface proteome analysis in primary neurons.

(B) Comparison of the surface proteomes of WT and S2KO primary neurons (mixed cortical-hippocampal cultures). n = 3 biological replicates/group (two technical replicates per biological replicate). Threshold applied: $\log_2$ratio(S2KO/WT) = ± 0.5; false discovery rate (FDR) = 0.15. See also Tables S2 and S3.

(C and D) JWA levels in brain lysates from WT ($S2^+$) and S2KO ($S2^-$) mice as shown by western blot analysis (C) and densitometric quantification thereof (D). N-cadherin served as loading control. Mean ± SEM. n = 6 mice per genotype. *p < 0.05 (unpaired t test). See also Figure S2.

(E and F) JWA mRNA levels in cortex (E) and hippocampus (hipp.) (F) of WT and S2KO mice as assessed by qRT-PCR (relative to actin). Mean ± SEM. n = 9 mice per genotype.

(G) SorCS2 (red) and EAAT3 (green) immunostainings on mouse brain sections (single confocal z planes). Sections are counterstained with DAPI. Insets show higher magnification of the overview pictures of cortex, dentate gyrus (DG), and CA2. Scale bars, 50 μm. See also Figure S3.

(H) SorCS2 (green) and EAAT3 (red) immunostainings in mouse hippocampal neurons (left) and C6 cells (right) (single confocal z planes). Cells are counterstained with DAPI. Higher magnification insets are shown. Scale bars, 10 μm.

(I) Co-immunoprecipitation (coIP) of EAAT3 with SorCS2-GFP (S2), but not β-galactosidase-GFP (βG), overexpressed in CHO cells. This experiment was replicated three times.

(J) coIP of EAAT3 with SorCS2 from mouse hippocampal lysates. IgG, non-specific IgG; IP, immunoprecipitation. This experiment was replicated three times.

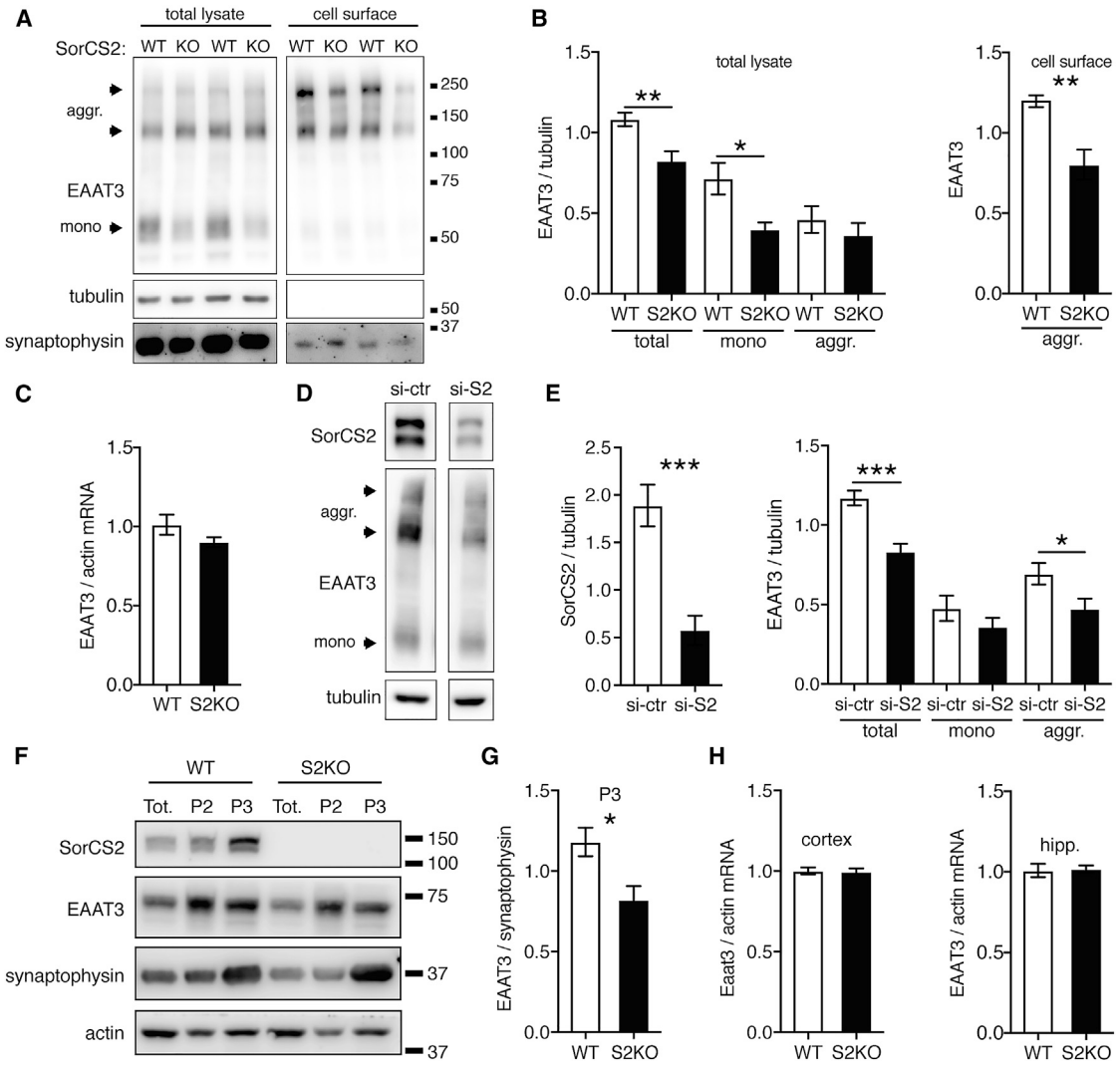

Figure 5. Loss of SorCS2 Leads to Missorting of EAAT3

(A and B) EAAT3 levels in total lysate and cell surface fractions of wild-type (WT) and S2KO (KO) neurons as shown by western blot analysis (A) and densitometric quantification thereof (B). Tubulin and synaptophysin served as loading controls. Tubulin is not present in cell surface fraction. EAAT3 monomers and aggregates are present in total neuronal lysates, while in the cell surface fraction, only aggregates are detected. Intensities of immunosignals from the indicated monomeric and aggregated forms of EAAT3 in the total lysates are shown separately, as well as combined (total). For the cell surface fraction, intensities of immunosignals from aggregated EAAT3 were quantified. Mean ± SEM. n = 7 independent neuronal preparations per genotype. *p < 0.05 and **p < 0.01 (unpaired t test).

(C) EAAT3 mRNA levels in WT and S2KO primary neurons as assessed by qRT-PCR (relative to actin mRNA). Mean ± SEM. n = 5 or 6 independent neuronal preparations per genotype.

(D and E) Levels of SorCS2 and EAAT3 in C6 cell lysates after SorCS2 knockdown (si-S2) as shown by western blot analysis (D) and densitometric quantification thereof (E). Intensities of immunosignals from the indicated monomeric and aggregated forms of EAAT3 are shown separately, as well as combined (total). Tubulin serves as loading control. Levels of aggregated and total EAAT3 are decreased after SorCS2 knockdown. Mean ± SEM. n = 9 independent transfection experiments. *p < 0.05 and ***p < 0.001 (unpaired t test).

(F) Levels of SorCS2 and EAAT3 in total lysate (Tot.) and in P2 and P3 fractions from WT and S2KO mouse brains. In tissue lysates and fractions, only monomeric EAAT3 is present. Synaptophysin and actin served as loading controls. See also Figure S4.

(G) Quantification of EAAT3 (monomer) levels in P3 fractions of WT and S2KO mouse brains (normalized to synaptophysin) as exemplified in (F). Mean ± SEM. n = 8 mice per genotype. *p < 0.05 (unpaired t test).

(H) EAAT3 mRNA levels in WT and S2KO cortices and hippocampi (hipp.) as assessed by qRT-PCR (relative to actin mRNA). Mean ± SEM. n = 9 mice per genotype.

In (A)–(C) mixed cortical-hippocampal cultures were used.

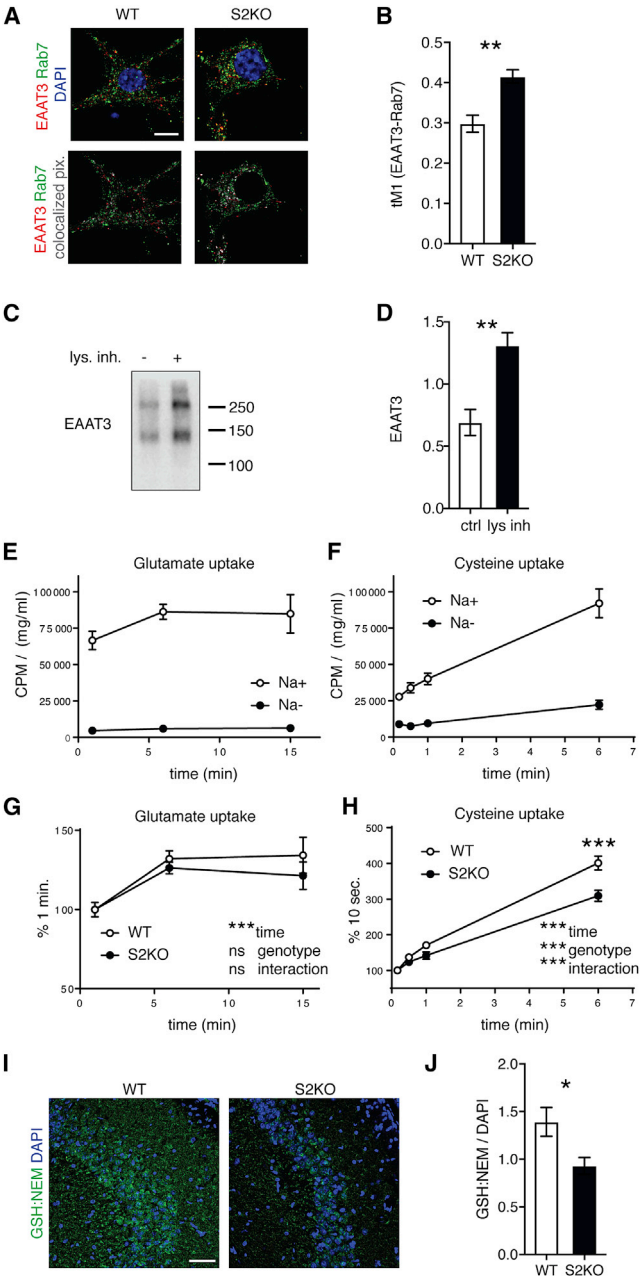

Figure 6. SorCS2 Deficiency Leads to Late Endosomal Sorting of EAAT3 and Disrupts Cysteine Import into Neurons

(A) Immunostaining of EAAT3 and Rab7 in primary WT and S2KO hippocampal neurons (single confocal z planes). Cells are counterstained with DAPI (blue). Bottom: colocalizing EAAT3 and Rab7-positive pixels are depicted in gray-scale. Scale bar, 10 μm.

(B) Extent of colocalization of EAAT3 and Rab7 in WT and S2KO neurons. tM1, fraction of EAAT3 overlapping with Rab7. Mean ± SEM. n = 10 neurons per genotype. **p < 0.01 (unpaired t test). This experiment was replicated three times.

(C) Western blot analysis of EAAT3 levels (two immunoreactive bands corresponding to aggregated forms) in the cell surface fraction of S2KO neurons under control conditions (lys. inh.$^-$) or after 2 h of treatment with lysosomal inhibitors (lys. inh.$^+$).

(D) Quantification of EAAT3 levels as exemplified in (C). Mean ± SEM. n = 5 independent neuronal preparations. **p < 0.01 (unpaired t test).

(E and F) [3H]-Glutamate (E) and [35S]-cysteine (F) uptake into primary WT neurons in Na-containing (Na$^+$) or Na-deprived (Na$^-$) buffer. Mean ± SEM.

(G) [3H]-Glutamate uptake into primary WT and S2KO neurons. Mean ± SEM. n = 7 or 8 independent neuronal preparations per genotype. ***p < 0.001 (two-way ANOVA).

(H) Na-dependent [35S]-cysteine uptake into primary WT and S2KO neurons. Mean ± SEM. n = 9 independent neuronal preparations per genotype. ***p < 0.001 (two-way ANOVA with Sidak's multiple-comparisons test).

(I) Immunostaining for glutathione:NEM adduct (GSH:NEM) (green) in CA2 regions of WT and S2KO mice. Sections were counterstained with DAPI (blue). Scale bar, 50 μm.

(J) GSH:NEM signal intensities (normalized to DAPI) in the CA2 regions of WT and S2KO mice as exemplified in (I). Mean ± SEM. n = 5 or 6 mice per genotype. *p < 0.05 (unpaired t test).

In (C)–(H) mixed cortical-hippocampal cultures were used.

DISCUSSION

The amino acid transporter EAAT3 is the main cysteine uptake route in neurons acting as a rate-limiting step for synthesis of the antioxidant glutathione. Although EAAT3 was initially described as a glutamate transporter, more recent evidence argues that its major activity is cysteine import as EAAT3-deficient mice show glutathione deficiency and age-related neurodegeneration (Aoyama et al., 2006). We now document a crucial function for the VPS10P domain receptor SorCS2 in controlling intracellular trafficking and cell surface activity of EAAT3 and the essential role of this sorting pathway for cysteine uptake and neuronal stress response.

Intracellular trafficking of EAAT3 has been studied extensively, identifying an exocytic and a recycling route taken by this transporter. The exocytic route is used by EAAT3 during biosynthesis and includes passage through endoplasmic reticulum and Golgi to the plasma membrane (Yang and Kilberg, 2002). By contrast, the recycling route is crucial for dynamic regulation of cell surface levels of EAAT3 and involves clathrin-dependent endocytosis followed by recycling through the Rab11$^+$ compartment back to the plasma membrane (González et al., 2007). Rab11$^+$ recycling endosomes are central for maintaining EAAT3 activity, as Rab11 dysfunction slows EAAT3 trafficking to the cell surface and impairs cysteine uptake and glutathione biosynthesis (Li et al., 2010).

We now uncovered a mechanism of SorCS2-mediated sorting of EAAT3 through Rab11$^+$ recycling compartments that is essential for efficient targeting of EAAT3 to the neuronal cell surface under normal and, importantly, under oxidative stress conditions. Our data are most consistent with a model whereby SorCS2 interacts with EAAT3 in Rab11$^+$ vesicles to sustain a recycling pool of EAAT3 that can dynamically mobilize transporter molecules to the cell surface to facilitate uptake of cysteine under stress conditions. In the absence of SorCS2, EAAT3 is aberrantly targeted to late endosomal compartments, depleting its recycling pool (i.e., P3 fraction) and, ultimately, reducing the amount of bioactive EAAT3 molecules at the neuronal cell surface. As a caveat, the anti-EAAT3 antiserum may exhibit different affinities for monomer versus aggregates of EAAT3 seen in lysates from primary neurons (Figures 5A and 6C) and C6 cells (Figure 5D). Thus, where applicable, we always quantified the total levels of EAAT3 but also monomers and aggregates

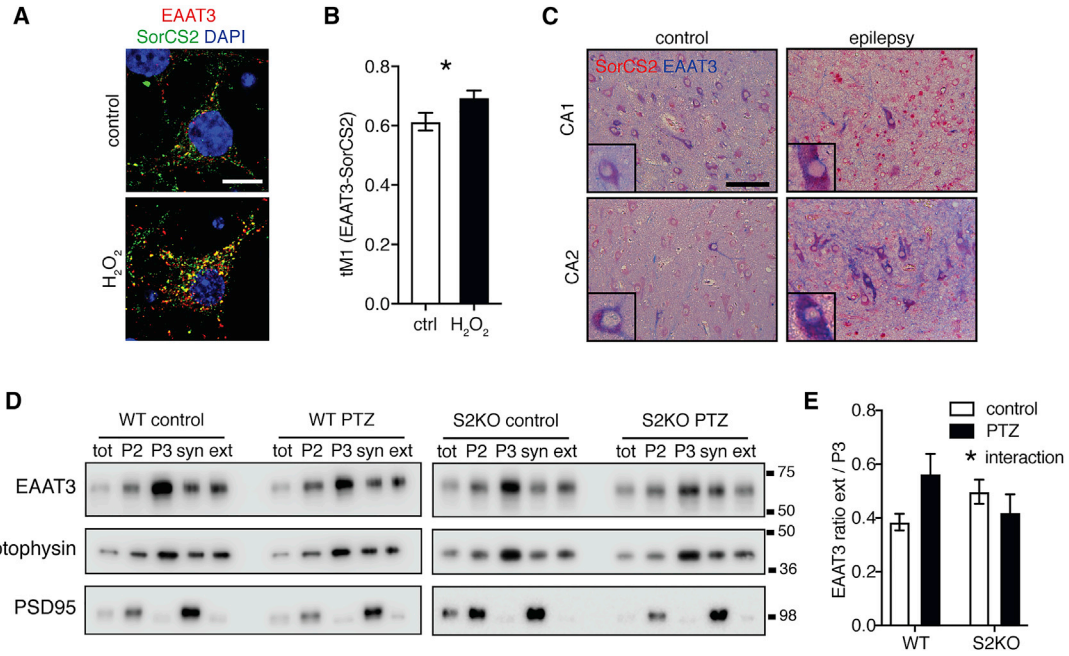

Figure 7. Subcellular Distribution of EAAT3 Is Dynamically Regulated during Epilepsy in a SorCS2-Dependent Manner

(A) Immunostaining of EAAT3 (red) and SorCS2 (green) in cultured WT neurons (mixed cortical-hippocampal culture) non-treated (control) or treated with 200 μM H_2O_2 for 30 min. Cells were counterstained with DAPI. Scale bar, 10 μm.

(B) Extent of colocalization of EAAT3 and SorCS2 in WT neurons under control conditions and after H_2O_2 treatment as exemplified in (A) (tM1, fraction of EAAT3 overlapping with SorCS2). Mean ± SEM. n = 10 neurons per condition. *p < 0.05 (unpaired t test). This experiment was replicated three times.

(C) Immunodetection of SorCS2 (red) and EAAT3 (blue) in CA1 and CA2 regions of the human control hippocampus and of the hippocampus of a patient with TLE and hippocampal sclerosis. Higher magnification insets are shown. Scale bar, 100 μm.

(D) Distribution of EAAT3 in subcellular brain fractions from WT and S2KO mice under basal conditions (control) or after PTZ kindling (PTZ). ext, extrasynaptic membranes; syn, synaptosomes; tot, total lysate. In tissue lysates and fractions, only monomeric EAAT3 is present. Synaptophysin and PSD95 were used as fraction markers.

(E) Ratio of EAAT3 (monomer) in extrasynaptic membranes (ext) versus P3 fractions from WT and S2KO mouse brains as exemplified in the western blot analysis in (D). A shift of EAAT3 from P3 to extrasynaptic membranes is seen in WT but not S2KO brains upon PTZ kindling. Mean ± SEM. n = 6 samples per group. *p < 0.05 (two-way ANOVA) for interaction.

separately to control for this possibility. In all experiments, both total levels as a well as the level of one form of EAAT3 were significantly reduced in samples lacking SorCS2. It remains unclear why in cell lysates from primary neurons it is the monomeric form but in C6 lysate the aggregated form of EAAT3 that shows a significant difference comparing genotypes, but most likely a different extent of EAAT3 aggregation in the two cell types explains this discrepancy. Importantly, this issue does not apply to experiments performed in mouse brain tissues, in which only monomeric EAAT3 is seen and significantly reduced in SorCS2 mutant mice (Figure 5F). Likely, the decrease in EAAT3 levels is caused by wrongful targeting of EAAT3 molecules to late endosomes, followed by lysosomal catabolism, as blockade of lysosomal activity rescues EAAT3 levels in SorCS2-deficient neurons. Although lysosomal degradation of EAAT3 is a physiological mechanism to regulate its turnover (Yang and Kilberg, 2002), this catabolic fate seems overrepresented in neurons lacking the sorting function of SorCS2.

In neurons, glutamate and cysteine transport capacities are dynamically regulated by adjusting EAAT3 levels at the cell surface (Fournier et al., 2004; Guillet et al., 2005). In line with a regulatory role for SorCS2 in this dynamic EAAT3 response, we observed an increase in SorCS2 levels (Figures 3E and 3F) and enhanced EAAT3-SorCS2 colocalization (Figures 7A and 7B) in neurons upon oxidative stress. Also *in vivo*, in the epileptic brains of humans and mouse models, we observed a dynamic response of EAAT3 that coincided with increased levels of SorCS2 (Figures 1A, 1B, and 7C–7E). Oxidative stress activates protein kinase C (PKC) (Gopalakrishna and Jaken, 2000), a potent regulator of plasma membrane exposure of EAAT3 (Fournier et al., 2004). Whether PKC promotes cell surface sorting of EAAT3 by increasing the activity of SorCS2 is not known, but PKC activation was shown to induce phosphorylation of the related VPS10P domain receptor SORLA (Lane et al., 2010).

Our data document that SorCS2 is crucial for protection against oxidative damage and neuronal cell death in the PTZ kindling model of epilepsy. Oxidative stress is a hallmark of epilepsy-driven pathology and represents a major process underlying the damaging effects of epileptic activity in the brain (Martinc et al., 2014). Increased levels of oxidative stress have been observed in virtually all epilepsy models (Shin et al., 2011) and in epileptic human brains (López et al., 2007). Increased oxidative damage and cell death in SorCS2-deficient mice coincided with accelerated mortality. The causal link between oxidative damage

and cell death with seizure-related mortality in the S2KO mouse model remains to be corroborated. However, there is ample evidence for a causative role of oxidative brain damage in mortality as treatment with antioxidants reduces oxidative stress and improves survival in epilepsy models (Pauletti et al., 2017).

Obviously, our present studies do not exclude that impairment of other neuronal activities of SorCS2, such as sorting of NMDA receptors (Ma et al., 2017) or control of neurotrophin signaling (Anastasia et al., 2013; Deinhardt et al., 2011; Glerup et al., 2016), may contribute to the increased sensitivity of mutant mice to seizure-induced mortality. However, loss of the dynamic response of EAAT3 to PTZ kindling (Figures 7D and 7E) strongly argues for impaired cysteine uptake as a molecular cause of enhanced oxidative stress and neuronal cell loss and associated mortality in epileptic S2KO mice. This notion receives further support from findings that levels and localization of EAAT3 are altered in animal models of epilepsy and in the human epileptic hippocampus (Crino et al., 2002).

Intriguingly, the functional interaction of SorCS2 with EAAT3 in protection from oxidative stress may not be restricted to epilepsy but be relevant for multiple brain pathologies, explaining the association of this receptor with psychiatric and neurodegenerative diseases (Baum et al., 2008; Christoforou et al., 2011; Ollila et al., 2009; Reitz et al., 2013). For example, altered brain levels or localization of EAAT3 were also reported in patients suffering from schizophrenia (Bauer et al., 2008) and Alzheimer's disease (Duerson et al., 2009). Also, in mouse models of Huntington's disease, both impaired SorCS2 function (Ma et al., 2017) and aberrant EAAT3 localization leading to increased oxidative stress (Li et al., 2010) were reported.

STAR★METHODS

Detailed methods are provided in the online version of this paper and include the following:

- KEY RESOURCES TABLE
- CONTACT FOR REAGENTS AND RESOURCE SHARING
- EXPERIMENTAL MODEL AND SUBJECT DETAILS
  - Human subjects
  - Mouse model
  - Neuronal cultures
  - Cell lines
- METHOD DETAILS
  - Plasmids, oligonucleotides, and cell transfections
  - Neuronal treatments
  - Purification of neuronal cell surface proteins
  - Mass spectrometry analysis of neuronal cell surface proteins
  - PTZ kindling procedure
  - Immunohistochemistry on human tissue
  - Immunohistochemistry on mouse tissue and cultured cells
  - Tissue fractionation
  - Immunoprecipitations
  - Western blot
  - Quantitative RT–PCR
  - Cysteine and glutamate uptake assays
- QUANTIFICATION AND STATISTICAL ANALYSIS
  - Image quantification
  - Statistical analysis

SUPPLEMENTAL INFORMATION

Supplemental Information can be found with this article online at https://doi.org/10.1016/j.celrep.2019.02.027.

ACKNOWLEDGMENTS

We are indebted to Jasper J. Anink, Andra Eisenmann, Tatjana Pasternack, Kristin Kampf, and Maria Kahlow for expert technical assistance. This work was supported by grants from the European Research Council (BeyOND 335692 to T.E.W.); the Helmholtz Association (AMPro to T.E.W.); the Berlin Institute of Health (Collaborative Research Group 11220008, to T.E.W.); the European Union's Seventh Framework Programme (FP7/2007-2013, grant agreement 602102, EPITARGET, to E.A. and K.L.); the European Union's Horizon 2020 Research and Innovation Programme (Marie Sklodowska-Curie grant agreement 722053, EU-GliaPhD, to E.A.); and Polish Ministry of Science and Education grant W19/7.PR/2014 (to K.L.).

AUTHOR CONTRIBUTIONS

Conceptualization, A.R.M., T.E.W., K.L., and E.A.; Methodology, A.R.M. and G.D.; Investigations, A.R.M., A.A., K.S., K.N., E.A.V., O.P., G.D., R.F.-G.; Writing of the Manuscript, A.R.M. and T.E.W.; Funding Acquisition, T.E.W., E.A., and K.L.; Resources, A.N.; Supervision, A.R.M., T.E.W., K.L., E.A., and J.A.K.

DECLARATION OF INTERESTS

The authors declare no competing interests.

Received: June 27, 2018
Revised: January 20, 2019
Accepted: February 7, 2019
Published: March 5, 2019

REFERENCES

Anastasia, A., Deinhardt, K., Chao, M.V., Will, N.E., Irmady, K., Lee, F.S., Hempstead, B.L., and Bracken, C. (2013). Val66Met polymorphism of BDNF alters prodomain structure to induce neuronal growth cone retraction. Nat. Commun. *4*, 2490.

Andersen, O.M., Reiche, J., Schmidt, V., Gotthardt, M., Spoelgen, R., Behlke, J., von Arnim, C.A.F., Breiderhoff, T., Jansen, P., Wu, X., et al. (2005). Neuronal sorting protein-related receptor sorLA/LR11 regulates processing of the amyloid precursor protein. Proc. Natl. Acad. Sci. U S A *102*, 13461–13466.

Aoyama, K., Suh, S.W., Hamby, A.M., Liu, J., Chan, W.Y., Chen, Y., and Swanson, R.A. (2006). Neuronal glutathione deficiency and age-dependent neurodegeneration in the EAAC1 deficient mouse. Nat. Neurosci. *9*, 119–126.

Aronica, E., Gorter, J.A., Ijlst-Keizers, H., Rozemuller, A.J., Yankaya, B., Leenstra, S., and Troost, D. (2003). Expression and functional role of mGluR3 and mGluR5 in human astrocytes and glioma cells: opposite regulation of glutamate transporter proteins. Eur. J. Neurosci. *17*, 2106–2118.

Bauer, D., Gupta, D., Harotunian, V., Meador-Woodruff, J.H., and McCullumsmith, R.E. (2008). Abnormal expression of glutamate transporter and transporter interacting molecules in prefrontal cortex in elderly patients with schizophrenia. Schizophr. Res. *104*, 108–120.

Baum, A.E., Akula, N., Cabanero, M., Cardona, I., Corona, W., Klemens, B., Schulze, T.G., Cichon, S., Rietschel, M., Nöthen, M.M., et al. (2008). A genome-wide association study implicates diacylglycerol kinase eta (DGKH) and several other genes in the etiology of bipolar disorder. Mol. Psychiatry *13*, 197–207.

Becker, A., Grecksch, G., Rüthrich, H.L., Pohle, W., Marx, B., and Matthies, H. (1992). Kindling and its consequences on learning in rats. Behav. Neural Biol. *57*, 37–43.

Berent-Spillson, A., and Russell, J.W. (2007). Metabotropic glutamate receptor 3 protects neurons from glucose-induced oxidative injury by increasing intracellular glutathione concentration. J. Neurochem. *101*, 342–354.

Blümcke, I., Thom, M., Aronica, E., Armstrong, D.D., Bartolomei, F., Bernasconi, A., Bernasconi, N., Bien, C.G., Cendes, F., Coras, R., et al. (2013). International consensus classification of hippocampal sclerosis in temporal lobe epilepsy: a Task Force report from the ILAE Commission on Diagnostic Methods. Epilepsia *54*, 1315–1329.

Chen, Y., and Swanson, R.A. (2003). The glutamate transporters EAAT2 and EAAT3 mediate cysteine uptake in cortical neuron cultures. J. Neurochem. *84*, 1332–1339.

Chen, R., Qiu, W., Liu, Z., Cao, X., Zhu, T., Li, A., Wei, Q., and Zhou, J. (2007). Identification of JWA as a novel functional gene responsive to environmental oxidative stress induced by benzo[a]pyrene and hydrogen peroxide. Free Radic. Biol. Med. *42*, 1704–1714.

Christoforou, A., McGhee, K.A., Morris, S.W., Thomson, P.A., Anderson, S., McLean, A., Torrance, H.S., Le Hellard, S., Pickard, B.S., StClair, D., et al. (2011). Convergence of linkage, association and GWAS findings for a candidate region for bipolar disorder and schizophrenia on chromosome 4p. Mol. Psychiatry *16*, 240–242.

Conti, F., DeBiasi, S., Minelli, A., Rothstein, J.D., and Melone, M. (1998). EAAC1, a high-affinity glutamate tranporter, is localized to astrocytes and gabaergic neurons besides pyramidal cells in the rat cerebral cortex. Cereb. Cortex *8*, 108–116.

Crino, P.B., Jin, H., Shumate, M.D., Robinson, M.B., Coulter, D.A., and Brooks-Kayal, A.R. (2002). Increased expression of the neuronal glutamate transporter (EAAT3/EAAC1) in hippocampal and neocortical epilepsy. Epilepsia *43*, 211–218.

Danbolt, N.C., Zhou, Y., Furness, D.N., and Holmseth, S. (2016). Strategies for immunohistochemical protein localization using antibodies: What did we learn from neurotransmitter transporters in glial cells and neurons. Glia *64*, 2045–2064.

Deinhardt, K., Kim, T., Spellman, D.S., Mains, R.E., Eipper, B.A., Neubert, T.A., Chao, M.V., and Hempstead, B.L. (2011). Neuronal growth cone retraction relies on proneurotrophin receptor signaling through Rac. Sci. Signal. *4*, ra82.

Dingledine, R., Varvel, N.H., and Dudek, F.E. (2014). When and how do seizures kill neurons, and is cell death relevant to epileptogenesis? Adv. Exp. Med. Biol. *813*, 109–122.

Duerson, K., Woltjer, R.L., Mookherjee, P., Leverenz, J.B., Montine, T.J., Bird, T.D., Pow, D.V., Rauen, T., and Cook, D.G. (2009). Detergent-insoluble EAAC1/EAAT3 aberrantly accumulates in hippocampal neurons of Alzheimer's disease patients. Brain Pathol. *19*, 267–278.

Escartin, C., Won, S.J., Malgorn, C., Auregan, G., Berman, A.E., Chen, P.-C., Déglon, N., Johnson, J.A., Suh, S.W., and Swanson, R.A. (2011). Nuclear factor erythroid 2-related factor 2 facilitates neuronal glutathione synthesis by upregulating neuronal excitatory amino acid transporter 3 expression. J. Neurosci. *31*, 7392–7401.

Fournier, K.M., González, M.I., and Robinson, M.B. (2004). Rapid trafficking of the neuronal glutamate transporter, EAAC1: evidence for distinct trafficking pathways differentially regulated by protein kinase C and platelet-derived growth factor. J. Biol. Chem. *279*, 34505–34513.

Glerup, S., Olsen, D., Vaegter, C.B., Gustafsen, C., Sjoegaard, S.S., Hermey, G., Kjolby, M., Molgaard, S., Ulrichsen, M., Boggild, S., et al. (2014). SorCS2 regulates dopaminergic wiring and is processed into an apoptotic two-chain receptor in peripheral glia. Neuron *82*, 1074–1087.

Glerup, S., Bolcho, U., Mølgaard, S., Bøggild, S., Vaegter, C.B., Smith, A.H., Nieto-Gonzalez, J.L., Ovesen, P.L., Pedersen, L.F., Fjorback, A.N., et al. (2016). SorCS2 is required for BDNF-dependent plasticity in the hippocampus. Mol. Psychiatry *21*, 1740–1751.

González, M.I., Kazanietz, M.G., and Robinson, M.B. (2002). Regulation of the neuronal glutamate transporter excitatory amino acid carrier-1 (EAAC1) by different protein kinase C subtypes. Mol. Pharmacol. *62*, 901–910.

González, M.I., Susarla, B.T.S., Fournier, K.M., Sheldon, A.L., and Robinson, M.B. (2007). Constitutive endocytosis and recycling of the neuronal glutamate transporter, excitatory amino acid carrier 1. J. Neurochem. *103*, 1917–1931.

Gopalakrishna, R., and Jaken, S. (2000). Protein kinase C signaling and oxidative stress. Free Radic. Biol. Med. *28*, 1349–1361.

Guillet, B.A., Velly, L.J., Canolle, B., Masmejean, F.M., Nieoullon, A.L., and Pisano, P. (2005). Differential regulation by protein kinases of activity and cell surface expression of glutamate transporters in neuron-enriched cultures. Neurochem. Int. *46*, 337–346.

Hermey, G., Plath, N., Hübner, C.A., Kuhl, D., Schaller, H.C., and Hermans-Borgmeyer, I. (2004). The three sorCS genes are differentially expressed and regulated by synaptic activity. J. Neurochem. *88*, 1470–1476.

Lane, R.F., Gatson, J.W., Small, S.A., Ehrlich, M.E., and Gandy, S. (2010). Protein kinase C and rho activated coiled coil protein kinase 2 (ROCK2) modulate Alzheimer's APP metabolism and phosphorylation of the Vps10-domain protein, SorL1. Mol. Neurodegener. *5*, 62.

Li, X., Valencia, A., Sapp, E., Masso, N., Alexander, J., Reeves, P., Kegel, K.B., Aronin, N., and Difiglia, M. (2010). Aberrant Rab11-dependent trafficking of the neuronal glutamate transporter EAAC1 causes oxidative stress and cell death in Huntington's disease. J. Neurosci. *30*, 4552–4561.

Lin, C.I., Orlov, I., Ruggiero, A.M., Dykes-Hoberg, M., Lee, A., Jackson, M., and Rothstein, J.D. (2001). Modulation of the neuronal glutamate transporter EAAC1 by the interacting protein GTRAP3-18. Nature *410*, 84–88.

Lionel, A.C., Crosbie, J., Barbosa, N., Goodale, T., Thiruvahindrapuram, B., Rickaby, J., Gazzellone, M., Carson, A.R., Howe, J.L., Wang, Z., et al. (2011). Rare copy number variation discovery and cross-disorder comparisons identify risk genes for ADHD. Sci. Transl. Med. *3*, 95ra75.

López, J., González, M.E., Lorigados, L., Morales, L., Riverón, G., and Bauzá, J.Y. (2007). Oxidative stress markers in surgically treated patients with refractory epilepsy. Clin. Biochem. *40*, 292–298.

Ma, Q., Yang, J., Milner, T.A., Vonsattel, J.G., Palko, M.E., Tessarollo, L., and Hempstead, B.L. (2017). SorCS2-mediated NR2A trafficking regulates motor deficits in Huntington's disease. JCI Insight *2*, 88995.

Martinc, B., Grabnar, I., and Vovk, T. (2014). Antioxidants as a preventive treatment for epileptic process: a review of the current status. Curr. Neuropharmacol. *12*, 527–550.

Mazella, J., Pétrault, O., Lucas, G., Deval, E., Béraud-Dufour, S., Gandin, C., El-Yacoubi, M., Widmann, C., Guyon, A., Chevet, E., et al. (2010). Spadin, a sortilin-derived peptide, targeting rodent TREK-1 channels: a new concept in the antidepressant drug design. PLoS Biol. *8*, e1000355.

Offe, K., Dodson, S.E., Shoemaker, J.T., Fritz, J.J., Gearing, M., Levey, A.I., and Lah, J.J. (2006). The lipoprotein receptor LR11 regulates amyloid beta production and amyloid precursor protein traffic in endosomal compartments. J. Neurosci. *26*, 1596–1603.

Ollila, H.M., Soronen, P., Silander, K., Palo, O.M., Kieseppä, T., Kaunisto, M.A., Lönnqvist, J., Peltonen, L., Partonen, T., and Paunio, T. (2009). Findings from bipolar disorder genome-wide association studies replicate in a Finnish bipolar family-cohort. Mol. Psychiatry *14*, 351–353.

Pauletti, A., Terrone, G., Shekh-Ahmad, T., Salamone, A., Ravizza, T., Rizzi, M., Pastore, A., Pascente, R., Liang, L.-P., Villa, B.R., et al. (2017). Targeting oxidative stress improves disease outcomes in a rat model of acquired epilepsy. Brain *140*, 1885–1899.

Reitz, C., Tosto, G., Vardarajan, B., Rogaeva, E., Ghani, M., Rogers, R.S., Conrad, C., Haines, J.L., Pericak-Vance, M.A., Fallin, M.D., et al.; Alzheimer's Disease Genetics Consortium (ADGC) (2013). Independent and epistatic effects of variants in VPS10-d receptors on Alzheimer disease risk and processing of the amyloid precursor protein (APP). Transl. Psychiatry *3*, e256.

Rohe, M., Hartl, D., Fjorback, A.N., Klose, J., and Willnow, T.E. (2013). SORLA-mediated trafficking of TrkB enhances the response of neurons to BDNF. PLoS ONE *8*, e72164.

Ruggiero, A.M., Liu, Y., Vidensky, S., Maier, S., Jung, E., Farhan, H., Robinson, M.B., Sitte, H.H., and Rothstein, J.D. (2008). The endoplasmic reticulum exit of glutamate transporter is regulated by the inducible mammalian Yip6b/GTRAP3-18 protein. J. Biol. Chem. *283*, 6175–6183.

Saadipour, K., Yang, M., Lim, Y., Georgiou, K., Sun, Y., Keating, D., Liu, J., Wang, Y.-R., Gai, W.-P., Zhong, J.-H., et al. (2013). Amyloid beta$_{1-42}$ (Aβ_{42}) up-regulates the expression of sortilin via the p75(NTR)/RhoA signaling pathway. J. Neurochem. *127*, 152–162.

Shin, E.-J., Jeong, J.H., Chung, Y.H., Kim, W.-K., Ko, K.-H., Bach, J.-H., Hong, J.-S., Yoneda, Y., and Kim, H.-C. (2011). Role of oxidative stress in epileptic seizures. Neurochem. Int. *59*, 122–137.

Steve, T.A., Jirsch, J.D., and Gross, D.W. (2014). Quantification of subfield pathology in hippocampal sclerosis: a systematic review and meta-analysis. Epilepsy Res. *108*, 1279–1285.

Su, J.-F., Wei, J., Li, P.-S., Miao, H.-H., Ma, Y.-C., Qu, Y.-X., Xu, J., Qin, J., Li, B.-L., Song, B.-L., et al. (2016). Numb directs the subcellular localization of EAAT3 through binding the YxNxxF motif. J. Cell Sci. *129*, 3104–3114.

Subkhangulova, A., Malik, A.R., Hermey, G., Popp, O., Dittmar, G., Rathjen, T., Poy, M.N., Stumpf, A., Beed, P.S., Schmitz, D., et al. (2018). SORCS1 and SORCS3 control energy balance and orexigenic peptide production. EMBO Rep. *19*, e44810.

Swiech, L., Blazejczyk, M., Urbanska, M., Pietruszka, P., Dortland, B.R., Malik, A.R., Wulf, P.S., Hoogenraad, C.C., and Jaworski, J. (2011). CLIP-170 and IQGAP1 cooperatively regulate dendrite morphology. J. Neurosci. *31*, 4555–4568.

Vaegter, C.B., Jansen, P., Fjorback, A.W., Glerup, S., Skeldal, S., Kjolby, M., Richner, M., Erdmann, B., Nyengaard, J.R., Tessarollo, L., et al. (2011). Sortilin associates with Trk receptors to enhance anterograde transport and neurotrophin signaling. Nat. Neurosci. *14*, 54–61.

Valavanidis, A., Vlachogianni, T., and Fiotakis, C. (2009). 8-hydroxy-2′ -deoxyguanosine (8-OHdG): A critical biomarker of oxidative stress and carcinogenesis. J Environ Sci Health C Environ Carcinog Ecotoxicol Rev *27*, 120–139.

VonDran, M.W., LaFrancois, J., Padow, V.A., Friedman, W.J., Scharfman, H.E., Milner, T.A., and Hempstead, B.L. (2014). p75NTR, but not proNGF, is upregulated following status epilepticus in mice. ASN Neuro. *6*, 1759091414552185.

Wang, D., Chan, C.-C., Cherry, S., and Hiesinger, P.R. (2013). Membrane trafficking in neuronal maintenance and degeneration. Cell. Mol. Life Sci. *70*, 2919–2934.

Watabe, M., Aoyama, K., and Nakaki, T. (2008). A dominant role of GTRAP3-18 in neuronal glutathione synthesis. J. Neurosci. *28*, 9404–9413.

Willnow, T.E., Petersen, C.M., and Nykjaer, A. (2008). VPS10P-domain receptors - regulators of neuronal viability and function. Nat. Rev. Neurosci. *9*, 899–909.

Yang, W., and Kilberg, M.S. (2002). Biosynthesis, intracellular targeting, and degradation of the EAAC1 glutamate/aspartate transporter in C6 glioma cells. J. Biol. Chem. *277*, 38350–38357.

STAR★METHODS

KEY RESOURCES TABLE

REAGENT or RESOURCE	SOURCE	IDENTIFIER
Antibodies		
anti-actin	Abcam	Cat# ab8227; RRID:AB_2305186
anti-EAAT3	Cell Signaling	Cat# 14501
anti-EAAT3	Santa Cruz Biotechnology	Cat# SC7761; RRID:AB_2302065
anti-p-ERK	Cell Signaling	Cat# 4370; RRID:AB_2315112
anti-GAD67	EMD Millipore	Cat# MAB5406; RRID:AB_2278725
anti-GFP	MBL International	Cat# MBL598; RRID:AB_591816
anti-GFAP (Cy3-conj.)	Sigma-Aldrich	Cat# C9205; RRID:AB_476889
anti-GluA1	EMD Millipore	Cat# MAB2263; RRID:AB_1977459
anti-GluA2	EMD Millipore	Cat# MABN71; RRID:AB_10806492
anti-GSH:NEM	EMD Millipore	Cat# MAB3194; clone 8.1GSH; RRID:AB_94744
anti-HO-1	Cell Signaling	Cat# 70081
anti-JWA	Trans Genic	Cat# KR057; RRID:AB_1627138
anti-mGlur2/3	Novus Biologicals	Cat# NB300-124; RRID:AB_2113758
anti-PSD95	Cell Signaling	Cat# 3409; RRID:AB_1264242
anti-N-cadherin	Cell Signaling	Cat# 14215
anti-Rab5	Cell Signaling	Cat# 2143; RRID:AB_823625
anti-Rab7	Cell Signaling	Cat# 9367; RRID:AB_1904103
anti-Rab11	Cell Signaling	Cat# 5589; RRID:AB_10693925
anti-SorCS2	R&D Systems	Cat# AF4237; RRID:AB_2192264
anti-SorCS2	Lifespan Biosciences	Cat# LS-C501334
anti-synaptophysin	Synaptic Systems	Cat# 101011; RRID:AB_887824
anti-tubulin	EMD Millipore	Cat# CP06
anti-8OHdG (FITC-conj.)	Santa Cruz Biotechnology	Cat# SC93871
Biological Samples		
Human brain samples	Department of Neuropathology of the Academic Medical Center (AMC) Amsterdam, the Netherlands	N/A
Chemicals, Peptides, and Recombinant Proteins		
bicuculline	Abcam	Cat #ab120107
EZ-LinkSulfo-NHS-SS-Biotin	Thermo Fisher Scientific	Cat #21331
L-[35S]-cysteine	PerkinElmer	Cat# NEG022T001MC
L-[3,4-3H]-glutamic acid	PerkinElmer	Cat# NET490250UC
N-ethylmaleimide (NEM)	Thermo Fisher Scientific	Cat# 23030
pentylenetetrazol (PTZ)	Sigma	Cat# P6500-25G
Critical Commercial Assays		
In Situ Cell Death Detection Kit, Fluorescein (TUNEL)	Roche	Cat# 11684795910
Experimental Models: Cell Lines		
C6 rat glioma cell line	Culture Collections (UK)	Cat# 92090409
CHO cell line	ATCC	CCL-61
Experimental Models: Organisms/Strains		
Sorcs2−/− (S2KO) mice	Glerup et al., 2014	N/A

(*Continued on next page*)

Continued

REAGENT or RESOURCE	SOURCE	IDENTIFIER
Oligonucleotides		
Actb (actin)	Thermo Fisher Scientific	Cat# Mm02619580
Ar6ip5 (JWA)	Thermo Fisher Scientific	Cat# Mm00480826
Grm3 (mGlur3)	Thermo Fisher Scientific	Cat# Mm00725298
EAAT3	Thermo Fisher Scientific	Cat# Mm00436590
ON-TARGET plus SMART pool	Dharmacon	Cat# L-085157-02-0005
ON-TARGET plus non-targeting Pool	Dharmacon	Cat# D-001810-10-05
Recombinant DNA		
rat EAAT3	González et al., 2002	N/A
GFP-tagged β-Galactosidase	Swiech et al., 2011	N/A
SorCS2-GFP	Generated in-house	N/A
Other		
GFP-Trap_MA resin	Chromotek	Cat# gtma-20
Neutravidin agarose resin	Thermo Fisher Scientific	Cat# 29201

CONTACT FOR REAGENTS AND RESOURCE SHARING

Further information and requests for resources and reagents should be directed to and will be fulfilled by the lead contact Thomas Willnow (willnow@mdc-berlin.de).

EXPERIMENTAL MODEL AND SUBJECT DETAILS

Human subjects

The cases included in this study were obtained from the archives of the Department of Neuropathology of the Academic Medical Center (AMC) Amsterdam, the Netherlands. Hippocampal specimens from 6 patients undergoing surgery for drug-resistant TLE were examined. The tissue was obtained and used in accordance with the Declaration of Helsinki and the AMC Research Code provided by the Medical Ethics Committee. All cases were reviewed independently by two neuropathologists and the classification of hippocampal sclerosis was based on analysis of microscopic examination as described by the International League Against Epilepsy (Blümcke et al., 2013). Hippocampal control tissues were obtained during autopsy of age-matched individuals without a history of seizures or other neurological diseases (n = 6). Table S1 summarizes the clinical characteristics of patients and controls.

Mouse model

Mice with targeted disruption of *Sorcs2* (S2KO) were described before (Glerup et al., 2014). S2KO mice on an inbred C57BL/6N background were used. For *in vivo* studies, mouse strain was kept by breeding of heterozygous animals and the WT and S2KO littermates were used in experiments. Newborn mice for preparing neuronal cultures were obtained by breeding of homozygous WT (C57BL/6N) or S2KO animals.

PTZ kindling experiments were performed using male mice at the age of 8-12 weeks. In all the other studies, brain tissue was collected from the mice of both sexes at the age of 8-12 weeks.

All animal experimentation was performed in accordance with institutional guidelines following approval by the local authorities of the State of Berlin (X9012/12, O0120/13) and by the First Ethical Committee in Warsaw (209/2016).

Neuronal cultures

Primary hippocampal or mixed cortical-hippocampal neuronal cultures were prepared from newborn S2KO and WT mice (postnatal day 0-1) using enzymatic digestion with papain. For biochemical studies, cortical neurons were plated on plastic plates coated with poly-D-lysine (Corning BIOCOAT) at a density of 64,000 cells/cm^2 (biotinylation studies) or 83,000 cells/cm^2 (neuronal stimulation). For immunocytochemistry, hippocampal neurons were plated on glass coverslips coated with poly-D-lysine and laminin at a density of 25,000 cells/cm^2 and mixed cortical-hippocampal neurons were plated on glass coverslips coated with poly-D-lysine at a density of 57,000 cells/cm^2. Neurons were maintained in Neurobasal medium (Invitrogen) supplemented with B27, GlutaMAX, and penicillin/streptomycin (Invitrogen). Neuronal cultures were used for experiments at day *in vitro* (DIV)10-13.

Cell lines

The C6 rat glioma cell line was purchased from Culture Collections (UK). The cells were maintained in DMEM medium supplemented with 5% FBS and penicillin/streptomycin (Invitrogen). CHO cells were obtained from ATCC and grown in DMEM medium supplemented with 10% FBS and penicillin/streptomycin (Invitrogen).

METHOD DETAILS

Plasmids, oligonucleotides, and cell transfections

Plasmids encoding rat EAAT3 and GFP-tagged β-Galactosidase were gifts from Michael Robinson and Jacek Jaworski, respectively (González et al., 2002; Swiech et al., 2011). The plasmid encoding murine SorCS2 tagged with GFP at the C terminus was generated in-house. Lipofectamine ™ 2000 was used for transfection of cells.

For transient knockdown of SorCS2 expression, Dharmacon siRNA (ON-TARGET plus SMART pool, L-085157-02-0005) or non-targeting control siRNA were used (ON-TARGET plus non-targeting Pool D-001810-10-05). Cells were transfected with siRNAs using X-tremeGENE siRNA transfection reagent (Roche). Two days post transfection, cells were washed twice with TBS-Ca-Mg buffer (20 mM Tris pH 7.6, 150 mM NaCl, 0.5 mM $MgCl_2$, 1 mM $CaCl_2$) and scraped in the lysis buffer containing 20 mM Tris pH 7.5, 150 mM NaCl, 2 mM EDTA, 0.5% Triton-X, 0.5% NP40, 2 mM MgCl2, 10% glycerol, and protease and phosphatase inhibitors. The lysate was kept on ice for 30 minutes and centrifuged for 10 minutes to collect the supernatant. Protein content was measured by BCA and samples were further prepared for western blot by adding Laemmli buffer and boiling.

Neuronal treatments

Neuronal cultures (mixed cortical-hippocampal) at DIV 10-12 were used. For H_2O_2 treatment, H_2O_2 was added to the conditioned cell culture medium at a final concentration of 200 μM and cells were incubated for 0.5, 3, 6 or 16 hours at 37°C. In case of bicuculline treatment, bicuculline (Abcam) was added to the conditioned cell culture medium at a final concentration of 20 μM and cells were incubated for 30 minutes at 37°C. Control cells were left untreated. After the stimulation, cell culture plates were placed on ice and washed 2 times with ice-cold TBS-Ca-Mg buffer. Next, neurons were scraped in lysis buffer containing 20 mM Tris pH 7.5, 150 mM NaCl, 2 mM EDTA, 0.5% Triton-X, 0.5% NP40, 2 mM $MgCl_2$, 10% glycerol, and protease and phosphatase inhibitors. The lysate was centrifuged (16,100x *g*, 15 min) to remove cell debris. The protein content was measured by BCA method and samples were prepared for western blotting. If the cells were used for immunostainings, they were fixed with 4%PFA/PBS after the stimulation.

To block lysosome function, the culture medium was supplemented with pepstatin (10 μM), leupeptin (100 μM), and chloroquine (50 μM), and the cells were incubated for 2 hours at 37°C prior to cell surface biotinylation.

Purification of neuronal cell surface proteins

Mixed cortical-hippocampal neuronal cultures prepared from newborn WT or S2KO mice were plated on poly-D-lysine-coated plates and cell surface biotinylation was performed at DIV10-12. To do so, cells were cooled down on ice for 15 min and washed 3 times with PBS-Mg-Ca (PBS supplemented with 0.5 mM $MgCl_2$ and 1 mM $CaCl_2$). Next, cells were incubated on ice with EZ-Link Sulfo-NHS-SS-Biotin solution (Thermo Fisher Scientific; 0.5 mg/ml in PBS) for 25 min, washed 3 times with quenching buffer (40 mM glycine, 0.4% BSA in TBS-Ca-Mg) and 2 times with TBS-Ca-Mg. Cells were scraped in lysis buffer (50 mM Tris pH 7.5, 1 mM EDTA, 2 mM EGTA, 150 mM NaCl, 1% NP40, 0.5% DOC, 0.1% SDS, protease and phosphatase inhibitors) and the lysates were rotated for 1.5 hours at 4°C. After centrifugation (15 min, 14,000x *g*), the supernatants were used for pull down of biotinylated proteins with NeutrAvidin slurry (Thermo Fisher Scientific). Equal amounts of proteins were loaded on the slurry. After washing 3 times with lysis buffer, the beads were snap-frozen and stored at −80°C until mass spectrometry analysis or boiled in Laemmli buffer to release captured proteins for western blot analysis.

Mass spectrometry analysis of neuronal cell surface proteins

Mass spectrometry analysis was performed as described (Subkhangulova et al., 2018). Samples containing biotinylated cell surface proteins were run on a stacking SDS-PAGE collecting all proteins in a single band. After Coomassie staining, the gel pieces were minced and digested with trypsin using a PAL robot (Axel Semrau/CTC Analytics). Peptides were extracted with extraction buffer (80% acetonitrile, 0.1% [v/v] formic acid) and dried in a speed-vac, followed by purification on C_{18} stage-tips. The eluted peptides were dried in a speed-vac and resuspended in 3% acetonitrile, 0.1% (v/v) formic acid.

The samples were measured by LC-MS/MS on a Q-Exactive Plus mass spectrometer (Thermo) connected to a Proxeon easy-nLC system (Thermo). The peptides were separated on an in-house prepared nano-LC column (0.074 mm × 250 mm, 3 μm Reprosil C_{18}, Dr Maisch GmbH) using a flow rate of 0.25 μl/min. MS acquisition was performed at a resolution of 70,000 in the scan range from 300 to 1,700 m/z. MS2 scans were carried out at a resolution of 15,500 with the isolation window of 2.0 m/z. Dynamic exclusion was set to 30 s, and the normalized collision energy was specified to 26.

For analysis, the MaxQuant software package version 1.5.2.8 was used. An FDR of 0.01 was applied for peptides and proteins, and the Andromeda search was performed using a mouse Uniprot database (August 2014). MS intensities were normalized by the MaxLFQ algorithm implemented in MaxQuant. MaxLFQ-normalized intensities among the replicates of the two groups to be related were used for statistical comparison. Decoy hits, contaminants and proteins that have only been identified by a site have been filtered

out from the resulting protein groups table. Proteins were further filtered for at least 2 valid values in one group before Welch t test was applied. Resulting *p-value*s were adjusted using the Benjamini-Hochberg procedure with an FDR-cutoff of 0.15. Further cutoff was applied on the $\log_2$ratio(S2KO/WT) level with values greater than 0.5 or lower than −0.5 considered as enriched. For data visualization, the $-\log_{10}$(p-value) was plotted against the $\log_2$ratio(S2KO/WT) using R (http://www.r-project.org). For better visualization, for proteins detected in either S2KO or WT samples only, the $\log_2$ratio(S2KO/WT) was set to 10 or −10, respectively.

PTZ kindling procedure

For up to 5 weeks, mice were intraperitoneally injected with subconvulsive doses (40 mg/kg body weight) of pentylenetetrazol (PTZ) in saline between 9:00 and 11:00 a.m. three times a week as described (Becker et al., 1992). After each injection, the convulsive behavior was video recorded for 30 min and the resultant seizures were scored as follows: stage 0, no response; stage 1, ear and facial twitching; stage 2, convulsive waves axially through the body; stage 3, myoclonic jerks and rearing; stage 4, turning over onto the lateral position; stage 5, turning over into the back and generalized tonic-clonic seizures and 6, for animals that died during the seizure. Latency from PTZ injection to seizure and the number of seizures in each session were also scored. The animals were considered to be kindled after having had at least three consecutive sessions when they reached stage 5 seizures. After completion of the experiment (15 sessions) or when animals died during the seizure, their brains were snap frozen on dry ice.

Immunohistochemistry on human tissue

Human brain tissue was fixed in 10% buffered formalin and embedded in paraffin. Paraffin-embedded tissue was sectioned at 5 μm, mounted on pre-coated glass slides (Star Frost, Waldemar Knittel) and processed for immunohistochemical staining. Sections were deparaffinated in xylene, rinsed in ethanol (100%, 95%, 70%), and incubated for 20 minutes in 0.3% hydrogen peroxide diluted in methanol. Antigen retrieval was performed using a pressure cooker in 10 mM sodium citrate, pH 6.0 at 120°C for 10 minutes. Slides were washed with phosphate-buffered saline (PBS; 0.1 M, pH 7.4) and incubated overnight with primary antibody (rabbit anti-SorCS2, Lifespan Biosciences, LS-C501334, 1:450) in Normal Antibody Diluent (Immunologic, Duiven, the Netherlands) at 4°C. After washing in PBS, sections were stained with a polymer-based peroxidase immunohistochemistry detection kit (Brightvision plus kit, ImmunoLogic) according to the manufacturer's instructions. Staining was performed using Bright DAB substrate solution (ImmunoLogic, Duiven, the Netherlands). Sections were dehydrated in alcohol and xylene, and coverslipped.

For double-labeling of SorCS2 with EAAT3, rabbit anti-SorCS2 (Lifespan Biosciences, LS-C501334, 1:450) and rabbit anti-EAAT3 (Cell Signaling, #14501, 1:150) antibodies were used. Sections were incubated with Brightvision poly-alkaline phosphatase (AP)-anti-rabbit (Immunologic) for 30 minutes at room temperature, and then washed with PBS. AP activity was visualized with the AP substrate kit III Vector Blue (SK-5300, Vector laboratories Inc.). To remove the first primary antibody, sections were incubated at 121°C in citrate buffer (10 mM NaCi, pH 6,0) for 10 min. Incubation with the second primary antibody was performed overnight at 4°C. AP activity was visualized with the alkaline phosphatase substrate kit I Vector Red (SK-5100, Vector laboratories Inc.). Negative control sections incubated without the primary antibodies or with the primary antibodies, followed by heating treatment were essentially blank.

Immunohistochemistry on mouse tissue and cultured cells

Mouse brains were dissected from 8 to 12 weeks old mice intracardially perfused with phosphate-buffered saline (PBS) and 4% paraformaldehyde (PFA) in PBS. After post-fixation (PFA, overnight) and cryopreservation in 30% sucrose/PBS, brains were cut in 50 μm coronal sections using a sliding microtome. Free-floating sections were blocked in 1% horse serum in PBS and incubated with primary followed by secondary antibodies diluted in PBS, supplemented with 1% bovine serum albumin (BSA), 1% normal donkey serum (NDS) and 0.5% Triton-X.

After PTZ kindling experiments, mouse brains were dissected and rapidly frozen. Next, 25 μm coronal sections were cut using a cryostat, immediately mounted on glass slides, and kept at −20°C until further use. Prior to staining, the sections were thawed at room temperature for 30 min and fixed in 4% PFA/PBS for 30 min. Sections were blocked and incubated with antibodies as described for free-floating sections above. For detection of 8OHdG, the blocking buffer contained 10% NDS, 1% BSA, and 0.3% Triton-X in TBS-T (132 mM NaCl, 2.7 mM KCl, 25 mM Tris pH 7.5, 0.1% Tween-20) and antibodies were diluted in TBS-T.

TUNEL reaction was performed using a commercially available kit (Roche). Sections were thawed for 30 min at 4°C and fixed in 25% acetic acid in ethanol for 30 min at 4°C. Next, the sections were blocked with 2% BSA, 1.5% normal goat serum, 0.1% Triton-X in PBS, and subjected to TUNEL reaction as described in the manufacturer's manual.

To visualize glutathione, the sections were first incubated for 4 hours at 4°C in 10 mM *N*-ethylmaleimide (NEM)/PBS. After washing with PBS, the sections were incubated overnight at 4°C with anti-GSH:NEM antibody in PBS supplemented with 0.3% Trition-X. Next, they were washed and incubated for 2 hours at room temperature with fluorescently labeled secondary antibody.

C6 cells grown on glass coverslips were fixed with 4% PFA/PBS. Cultured neurons grown on glass coverslips were fixed with 4% PFA/PBS at DIV 10-12. Next, the cells were washed with PBS, blocked for 1 hour in PBS supplemented with 5% NDS and 0.3% Triton-X, and incubated with primary antibodies diluted in PBS with 1% BSA and 0.3% Triton-X.

Following antibodies were used for immunostainings: anti-EAAT3 (Cell Signaling, #14501, 1:100; Santa Cruz Biotechnology, SC7761, 1:100), anti-GAD67 (EMD Millipore, MAB5406, 1:100), anti-Rab5 (Cell Signaling, #2143, 1:100), anti-Rab7 (Cell Signaling, #9367, 1:100), anti-Rab11 (Cell Signaling, #5589, 1:100), anti-SorCS2 (R&D Systems, AF4237, 1:100), anti-GSH:NEM (Millipore, MAB3194, 1:100). Primary antibodies were visualized using Alexa Fluor 555, 488 or 647 secondary antibody conjugates. 8OHdG

was immunodetected using FITC-conjugated antibody (Santa Cruz Biotechnology, SC93871, 1:50) and GFAP was detected using Cy-3 conjugated antibody (Sigma-Aldrich C9205, 1:1,500).

The cells and tissue sections were counterstained with DAPI and mounted with DAKO fluorescence mounting medium.

Tissue fractionation

Brain subcellular fractionations were performed as illustrated on Figure S4A. Brain tissues (hippocampi and cortices) from 8 to 12 weeks old mice were used. For each preparation, tissue from 2 mice was pooled. Tissue was homogenized with glass homogenizer in Tris-buffered sucrose with Ca and Mg (0.32 M sucrose, 6 mM Tris, 1 mM $MgCl_2$, 0.5 mM $CaCl_2$, protease and phosphatase inhibitors, pH 8). The resulting suspension was centrifuged (1,400x g, 20 min) yielding the supernatant (S1a) and the pellet, that was homogenized again in Tris-buffered sucrose with Ca and Mg and centrifuged to remove nuclear debris (710x *g* 10 min) and to collect the supernatant (S1b). Supernatants S1a and S1b were combined to get a total lysate (S1) that was further centrifuged (13,800 × g, 30 min) to pellet the crude membrane fraction (P2). The resulting supernatant (S2) was subjected to ultracentrifugation (100,000 × g, 1 h) to yield the intracellular vesicles fraction (P3). The P2 fraction was homogenized in Tris-buffered sucrose (0.32 M sucrose, 6 mM Tris pH 8) and layered onto a discontinuous sucrose density gradient (0.85 M, 1.0 M, 1.2 M sucrose buffered with 6 mM Tris pH 8) and centrifuged (82,500x *g*, 2h) to recover the extrasynaptic membranes at the interphase between the layered P2 fraction and 0.85 M sucrose, and the synaptosomal fraction at the interphase between 1.0 M and 1.2 M sucrose. The synaptosomal fraction was further supplemented with Triton X-100 to a final concentration of 0.5%, and incubated on ice for 15 min. Further centrifugation (32,000x *g*, 20 min) pelleted the PSD1 fraction, that was resuspended in 40 mM Tris pH 8.

To obtain only P2 and P3 fractions, simplified protocol was used. Tissue (cortex and hippocampus, 1 hemi-brain per sample) was homogenized with glass homogenizer in a sucrose buffer containing 0.32M sucrose,10mM Tris-HCl (pH 7.5), 1mM EDTA and protease and phosphatase inhibitors. Homogenate was centrifuged at 1,000x *g* for 10 min to remove the nuclear fraction and tissue debris. Resulting supernatant (total lysate) was centrifuged at 10,000x *g* for 15 minutes to yield a crude membrane fraction (P2) and S2. Further centrifugation (100,000x *g*, 1 h) of S2 fraction pelleted the intracellular vesicles fraction (P3). P2 fraction was resuspended in sucrose buffer with 0.5% Triton X-100 and P3 fraction was resuspended in 10 mM Tris buffer.

Protein concentrations were measured for all the fractions and equal amounts of protein were loaded on an SDS-PAGE gel for western blot analysis.

Immunoprecipitations

Hippocampi from WT and S2KO mice were homogenized in lysis buffer containing 20 mM Tris pH 7.5, 150 mM NaCl, 1 mM $CaCl_2$, 1 mM $MgCl_2$, protease and phosphatase inhibitors, and kept on ice for 20 min. Next, the lysates were centrifuged (1,000x *g*, 10 min) and the tissue debris was discarded. CHAPS was added to the lysates to a final concentration of 0.6% and the lysates were rotated for 1 hour at 4°C. After centrifugation (16,100x *g,* 15 min), the supernatant was loaded on protein G agarose beads coupled to anti-SorCS2 antibody (R&D, AF4237) or to unspecific sheep IgG, rotated overnight and washed 3 times with lysis buffer supplemented with 0.3% CHAPS. Proteins bound to the resin were released by boiling in Laemmli buffer and analyzed by western blot.

Chinese hamster ovary (CHO) cells were transfected with expression constructs encoding rat EAAT3 and GFP-tagged β-Galactosidase or murine SorCS2 using Lipofectamine™ 2000 reagent (Invitrogen). Two days after transfection, cells were washed twice and scraped in TBS-Ca-Mg buffer, and centrifuged to obtain a cell pellet (16,100x *g*, 15 min). The cell pellet was resuspended in lysis buffer (20 mM Tris pH 7.5, 150 mM NaCl, 1 mM $MgCl_2$, 1 mM $CaCl_2$) supplemented with 0.6% CHAPS, and protease and phosphatase inhibitors. After shaking for 30 minutes on ice, the lysate was centrifuged to remove the cell debris (16,100x *g*, 15 min). The supernatant was applied to GFP Trap beads (Chromotek) for GFP immunoprecipitation. The samples were rotated for 1 hour at 4°C before the resin was washed 3 times with lysis buffer supplemented with 0.2% CHAPS. Proteins bound to the resin were released by boiling in Laemmli buffer and analyzed by western blot.

Western blot

Tissue and cell lysates were analyzed by western blot using the following antibodies: anti-SorCS2 (R&D Systems, AF4237, 1:1000), anti-EAAT3 (Cell Signaling, #14501, 1:1000), anti-p-ERK (Cell Signaling, #4370, 1:2000), anti-tubulin (EMD Millipore, CP06, 1:5000), anti-mGlur2/3 (Novus Biologicals, NB300-124, 1:1000), anti-actin (Abcam, ab8227, 1:2000), anti-JWA (Trans Genic, KR057, 1:250), anti-N-cadherin (Cell Signaling, #14215, 1:1000), anti-GFP (MBL International, MBL598, 1:2000), anti-Rab11 (Cell Signaling, #5589, 1:1000), anti-synaptophysin (Synaptic Systems, 101011, 1:5000), anti-GluA1 (EMD Millipore, MAB2263, 1:1000), anti-GluA2 (EMD Millipore, MABN71, 1:1000), anti-PSD95 (Cell Signaling, #3409, 1:1000), anti-HO-1 (Cell Signaling, #70081, 1:1000). After incubation with secondary antibodies coupled to HRP, chemiluminescent signal was registered with use of digital LI-COR imaging system.

Quantitative RT–PCR

Total RNA was extracted from tissue and cell lysates using TRIzol reagent and purified with RNeasy Mini Kit (QIAGEN). Reversely transcribed cDNA from total RNA was subjected to qRT–PCR using the following Taqman Gene Expression Assays: Actb (actin, Mm02619580), Ar6ip5 (JWA, Mm00480826), Grm3 (mGlur3, Mm00725298), EAAT3 (Mm00436590). Fold change in gene expression was calculated using the cycle threshold (CT) comparative method (2^{-}ddCT) normalizing to Actb CT values.

Cysteine and glutamate uptake assays

Cultures of mixed cortical-hippocampal neurons from WT and S2KO mice were used at DIV 10-13.

Cells were washed 3 times with warm assay buffer (5 mM Tris pH 7.5, 10 mM HEPES, pH 7.27, 2.5 mM KCl, 1.2 mM $CaCl_2$, 1.2 mM $MgCl_2$, 1.2 mM K_2HPO4, 10 mM glucose; 140 mM NaCl) and then incubated with the warm assay buffer containing L-[35S]-cysteine (0.005 uCi/ul, PerkinElmer), unlabeled L-cysteine (10 μM, Sigma-Aldrich) and DTT (100 μM, 1,4-Dithiothreitol, Sigma-Aldrich) or warm assay buffer containing L-[3,4-3H]-glutamic acid (100 nM, PerkinElmer) and unlabeled L-glutamic acid (10 μM, Sigma-Aldrich). To study Na-independent cysteine uptake, the sodium chloride in the assay buffer was replaced with choline chloride (Sigma-Aldrich,) and the pH was adjusted with KOH.

Cysteine uptake assays were performed at room temperature for 10, 30, 60, and 360 s. Glutamate uptake was performed at 37°C for 0.5, 1, 6, and 15 minutes. At indicated time points, cells were rapidly washed 3 times with cold Tris-Ca-Mg buffer followed by lysis. Cells were scraped in lysis buffer (50 mM Tris, pH 7.4, 140 mM NaCl, 1% Triton X-100) supplemented with protease inhibitor cocktail and incubated for 30 minutes on ice. Subsequently, the lysates were centrifuged at 13,400x *g* for 10 minutes and the supernatant was used for further analysis.

The radioactive cysteine and glutamic acid contents were determined in a Liquid Scintillation Analyzer (Tri-Carb 2800TR, PerkinElmer) using 10 μl of the supernatant sample in 4 mL of liquid scintillation cocktail (Rotiszint eco plus, Carl Roth).

Values were normalized to protein content and, in case of cysteine uptake, the values obtained for Na-independent cysteine uptake were subtracted from the total uptake. Finally, values were given relative to the value obtained for the earliest time point of the uptake experiment (set to 100%).

QUANTIFICATION AND STATISTICAL ANALYSIS

Image quantification

Western blot signals were quantified using the Image Studio Lite software. For quantification of multiple bands (monomers and aggregates), the bands intensities were quantified separately and next combined.

Microscopy images were quantified using Fiji software. Signal intensities were measured on single channel images as mean gray value for a selected area. Colocalization analysis for neuronal images was performed with Colocalization Threshold plugin with manual selection of the region of interest, covering neuronal cell soma and initial segments of primary dendrites. Single z-plane images were used for calculating Mander's coefficient (tM1).

To quantify the number of TUNEL-positive cells, the CA2/3 region was manually selected, color channels were separated, and threshold was applied to minimize the background signal. Next, DAPI-positive regions were used to mask the green channel (TUNEL) and TUNEL-positive particles were counted automatically.

The 8OHdG signal intensity was quantified in manually selected CA and DG regions after separating the channels and applying a threshold to minimize the background signal. For each set of tissue sections stained in parallel, intensities were normalized to a mean value obtained for the WT mice.

The GSH:NEM signal intensity was quantified along with DAPI signal intensity within a manually selected region containing CA2 neurons. The GSH:NEM signal measurement was further normalized to DAPI intensity in the same region.

Statistical analysis

For all *in vivo* experiments, an indicated number *n* is the number of mice per group used in an experiment. For neuronal culture experiments, an indicated number *n* is the number of independent neuronal preparations (biological replicates) used for western blot or qRT-PCR analysis. In case of colocalization studies, *n* is the number of individual cells quantified in a given experiment, and every experiment was replicated at least three times on independent neuronal cultures.

Each mouse (or biological replicate/individual cell in neuronal cell culture experiments) represents a statistically independent experimental unit, which was treated accordingly as an independent value in the statistical analyses. Statistical analyses were performed using GraphPad Prism software. For comparison between two experimental groups, a two-tailed unpaired t-test was used. PTZ kindling response was assayed with repeated-measures two-way ANOVA. Survival curve was analyzed using Gehan-Breslow-Wilcoxon test. For all other data with two independent variables (factors), two-way ANOVA with Sidak's multiple comparisons test was applied. Where applicable, outlier analysis was performed using Grubb's test. The details of statistical analysis are specified in the figure legends.

In mass spectrometry experiments, differences in protein levels were compared by Welch t test with Benjamini-Hochberg correction of *p-value*, with an FDR of 0.15.